Kondo quantum dot coupled to ferromagnetic leads: Numerical renormalization group study

M. Sindel,[1] L. Borda,[1,2] J. Martinek,[3,4,5] R. Bulla,[6] J. König,[7] G. Schön,[5] S. Maekawa,[3] and J. von Delft[1]
[1]*Physics Department, Arnold Sommerfeld Center for Theoretical Physics, and Center for NanoScience, Ludwig-Maximilians-Universität München, 80333 München, Germany*
[2]*Research Group "Theory of Condensed Matter" of the Hungarian Academy of Sciences, TU Budapest, Budapest H-1521, Hungary*
[3]*Institute for Materials Research, Tohoku University, Sendai 980-8577, Japan*
[4]*Institute of Molecular Physics, Polish Academy of Sciences, 60-179 Poznań, Poland*
[5]*Institut für Theoretische Festkörperphysik and DFG-Center for Functional Nanostructures (CFN), Universität Karlsruhe, D-76128 Karlsruhe, Germany*
[6]*Theoretische Physik III, Elektronische Korrelationen und Magnetismus, Universität Augsburg, D-86135 Augsburg, Germany*
[7]*Institut für Theoretische Physik III, Ruhr-Universität Bochum, 44780 Bochum, Germany*
(Received 18 July 2006; revised manuscript received 3 November 2006; published 18 July 2007)

We systematically study the influence of ferromagnetic leads on the Kondo resonance in a quantum dot tuned to the local moment regime. We employ Wilson's numerical renormalization group method, extended to handle leads with a spin asymmetric density of states, to identify the effects of (i) a finite spin polarization in the leads (at the Fermi surface), (ii) a Stoner splitting in the bands (governed by the band edges), and (iii) an arbitrary shape of the lead density of states. For a generic lead density of states, the quantum dot favors being occupied by a particular spin species due to exchange interaction with ferromagnetic leads, leading to suppression and splitting of the Kondo resonance. The application of a magnetic field can compensate this asymmetry, restoring the Kondo effect. We study both the gate voltage dependence (for a fixed band structure in the leads) and the spin polarization dependence (for fixed gate voltage) of this compensation field for various types of bands. Interestingly, we find that the full recovery of the Kondo resonance of a quantum dot in the presence of leads with an energy-dependent density of states is possible not only by an appropriately tuned external magnetic field but also via an appropriately tuned gate voltage. For flat bands, simple formulas for the splitting of the local level as a function of the spin polarization and gate voltage are given.

DOI: 10.1103/PhysRevB.76.045321 PACS number(s): 72.15.Qm, 75.20.Hr, 72.25.−b, 73.23.Hk

I. INTRODUCTION

The interplay between different many-body phenomena, such as superconductivity, ferromagnetism, or the Kondo effect, has recently attracted a lot of experimental and theoretical attention. A recent experiment of Buitelaar *et al.*[1] nicely demonstrated that Kondo correlations compete with superconductivity in the leads. The interplay between Kondo correlations and itinerant electron ferromagnetism in the electrodes has theoretically been intensively studied within the last years,[2–9] initially leading to controversial conclusions.

For effectively single-level quantum dots (i.e., dots with a level spacing much bigger than the level broadening Γ), consensus was found that a finite spin asymmetry in the density of states in the leads results (in general) in splitting and suppression of the Kondo resonance. This is due to the spin-dependent broadening and renormalization of the dot level position induced by spin-dependent quantum charge fluctuations. In terms of the Kondo spin model, it can be treated as an effective exchange interaction between a localized spin on the dot and ferromagnetic leads. Moreover, it was shown that a strong coupling Kondo fixed point with a reduced Kondo temperature can develop[6,7] even though the dot is coupled to ferromagnetic leads, given that an external magnetic field[6] or electric field[7] (gate voltage) is tuned appropriately. Obviously, in the limit of fully spin-polarized leads, when only one spin component is present for energies close to the Fermi surface (half-metallic leads), the effective screening of the impurity *cannot* take place any more and the Kondo resonance does *not* develop. A part of these theoretical predictions have recently been confirmed in an experiment by Pasupathy *et al.*[10] The presence of ferromagnetic leads could also nicely explain the experimental findings of Nygård *et al.*[11]

Since the interplay between ferromagnetism and strong correlation effects is one of the important issues in spintronic applications, there are currently many research activities going on in this direction. The goal is to manipulate the magnetization of a local quantum dot (i.e., its local spin) by means of an external parameter, such as an external magnetic field or an electric field (a gate voltage), with high accuracy. This would provide a possible method of writing information in a magnetic memory.[12] Since it is extremely difficult to confine a magnetic field such that it only affects the quantum dot under study, it is of big importance to search for alternative possibilities for such a manipulation (e.g., by means of a local gate voltage, as proposed by the authors[13]).

In this paper, we push forward our previous work by performing a systematic analysis on the dependence of physical quantities on different band structure properties. Starting from the simplest case, we add the ingredients of a realistic model one by one, allowing a deeper understanding of the interplay of the Kondo model and itinerant electron ferromagnetism. In this paper, we extend our recent studies carried out in this direction[6,7,13] and illustrate the strength of the analytical methods by comparing the results predicted by them to the results obtained by the exact numerical renormalization group (NRG) method.[14] While in Refs. 2–9 the dot was attached to ferromagnetic leads with an unrealistic, spin-

independent, and flat band—with a spin-dependent tunneling amplitude—we generalize this treatment here by allowing for arbitrary density of states (DOS) shapes.[13] In particular, we carefully analyze the consequences of typical DOS shapes in the leads on the Kondo resonance. We explain the difference between these shapes and provide simple formulas (based on perturbative scaling analysis[15,16]) that explain the numerical results analytically.

We study both the effect of a finite lead spin polarization and the gate voltage dependence of a single-level quantum dot contacted to ferromagnetic leads with three relevant DOS classes: (i) for flat bands without Stoner splitting, (ii) for flat bands with Stoner splitting and, (iii) for an energy-dependent DOS (also including Stoner splitting). For this sake, we employ an extended version of the NRG method to handle arbitrary shaped bands.[17]

The article is organized as follows: In Sec. II, we define the model Hamiltonian of the quantum dot coupled to ferromagnetic leads. In Sec. III, we explain details of the Wilson mapping on the semi-infinite chain in the case of the spin-dependent density of states with arbitrary energy dependence. Using the perturbative scaling analysis, we give prediction for a spin-splitting energy for various band shapes in Sec. IV. In Sec. V, the results for spin-dependent flat DOS are demonstrated, together with the Friedel sum rule analysis. The effect of the Stoner splitting is discussed in Sec. VI, together with comparison to experimental results from Ref. 11 and an arbitrary band structure in Sec. VII. We summarize our findings then in Sec. VIII.

II. MODEL: QUANTUM DOT COUPLED TO FERROMAGNETIC LEADS

We model the problem at hand by means of a single-level dot of energy ϵ_d (tunable via an external gate voltage V_G) and charging energy U that is coupled to identical, noninteracting leads (in equilibrium) with Fermi energy $\mu=0$. Accordingly, the system is described by the following Anderson impurity model:

$$\hat{\mathcal{H}} = \hat{\mathcal{H}}_\ell + \hat{\mathcal{H}}_{\ell d} + \hat{\mathcal{H}}_d,$$

$$\hat{\mathcal{H}}_d = \epsilon_d \sum_\sigma \hat{n}_\sigma + U\hat{n}_\uparrow \hat{n}_\downarrow - BS_z, \tag{1}$$

with the lead and the tunneling part of the Hamiltonian

$$\hat{\mathcal{H}}_\ell = \sum_{rk\sigma} \epsilon_{rk\sigma} c^\dagger_{rk\sigma} c_{rk\sigma}, \tag{2}$$

$$\hat{\mathcal{H}}_{\ell d} = \sum_{rk\sigma} (V_{rk} d^\dagger_\sigma c_{rk\sigma} + \text{H.c.}). \tag{3}$$

Here, $c_{rk\sigma}$ and d_σ ($\hat{n}_\sigma = d^\dagger_\sigma d_\sigma$) are the Fermi operators for electrons with momentum k and spin σ in lead r ($r=L/R$) and in the dot, respectively. The spin-dependent dispersion in lead r, parametrized by $\epsilon_{rk\sigma}$, reflects the spin-dependent DOS, $\rho_{r\sigma}(\omega) = \Sigma_k \delta(\omega - \epsilon_{rk\sigma})$, in lead r; *all* information about energy and spin dependency in lead r is contained in the dispersion function $\epsilon_{rk\sigma}$. V_{rk} labels the tunneling matrix element between the impurity and lead r, $S_z = (\hat{n}_\uparrow - \hat{n}_\downarrow)/2$, and the last term in Eq. (1) denotes the Zeeman energy due to external magnetic field B acting on the dot spin only. Here, we neglect the effect of an external magnetic field on the leads' electronic structure, as well as a stray magnetic field from the ferromagnetic leads. The coupling between the dot level and electrons in lead r leads to a broadening and a shift of the level ϵ_d, $\epsilon_d \to \tilde{\epsilon}_d$ (where the tilde denotes the renormalized level). The *energy* and *spin* dependency of the broadening and the shift, determined by the coupling, $\Gamma_{r\sigma}(\omega) = \pi \rho_{r\sigma}(\omega) |V_r(\omega)|^2$, plays the key role in the effects outlined in this paper. Henceforth, we assume V_{rk} to be real and k independent, $V_{rk\sigma} = V_r$, and lump all energy and spin dependence of $\Gamma_{r\sigma}(\omega)$ into the DOS in lead r, $\rho_{r\sigma}(\omega)$.[18]

Without loosing generality, we assume the coupling to be symmetric, $V_L = V_R$. Accordingly, by performing a unitary transformation,[19] $\hat{\mathcal{H}}_\ell$ simplifies to $\hat{\mathcal{H}}_\ell = \frac{1}{2}\Sigma_{k\sigma}(\epsilon_{Lk\sigma} + \epsilon_{Rk\sigma}) \alpha^\dagger_{sk\sigma} \alpha_{sk\sigma}$, where $\alpha_{sk\sigma}$ denotes the proper unitary combination of lead operators which couple to the quantum dot and we dropped the part of the lead Hamiltonian which is decoupled from the dot. With the help of the definitions $V \equiv \sqrt{V_L^2 + V_R^2}$, $\alpha_{k\sigma} \equiv \alpha_{sk\sigma}$, and $\epsilon^*_{k\sigma} \equiv \frac{1}{2}(\epsilon_{Lk\sigma} + \epsilon_{Rk\sigma})$, the full Hamiltonian can be cast into a compact form,

$$\hat{\mathcal{H}} = \sum_{k\sigma} \epsilon^*_{k\sigma} \alpha^\dagger_{k\sigma} \alpha_{k\sigma} + \sum_{k\sigma} V(d^\dagger_\sigma \alpha_{k\sigma} + \text{H.c.}) + \hat{\mathcal{H}}_d, \tag{4}$$

with $\hat{\mathcal{H}}_d$ as given in Eq. (1).

A. Ferromagnetic leads

For ferromagnetic materials, electron-electron interaction in the leads gives rise to magnetic order and spin-dependent DOS, $\rho_{r\uparrow}(\omega) \neq \rho_{r\downarrow}(\omega)$. Magnetic order of typical band ferromagnets such as Fe, Co, and Ni is mainly related to electron correlation effects in the relatively narrow $3d$ subbands, which only weakly hybridize with $4s$ and $4p$ bands.[20] We can assume that due to a strong spatial confinement of d electron orbitals, the contribution of electrons from d subbands to transport across the tunnel barrier can be neglected.[21] In such a situation, the system can be modeled by noninteracting[22] s electrons, which are spin polarized due to the exchange interaction with uncompensated magnetic moments of the completely localized d electrons. In mean-field approximation, one can model this exchange interaction as an effective molecular field, which removes spin degeneracy in the system of noninteracting conducting electrons, leading to a spin-dependent DOS.

In experiments, very frequently, the electronic transport measurements are performed for two configurations of the leads' magnetization direction:[10] the parallel and antiparallel alignments. By comparison of electric current for these two configurations, one can calculate the tunneling magnetoresistance, an important parameter for the application of the magnetic tunnel junction.[12]

In this paper, we restrict the leads' magnetization direction to be either (i) *parallel*, i.e., the left and right leads have the DOS $\rho_{L\sigma}(\omega)$ and $\rho_{R\sigma}(\omega)$, respectively, so the total DOS

corresponding to the total dispersion $\epsilon^*_{k\sigma}$ ($\forall k \in [-D_0;D_0]$) is given by $\rho_\sigma(\omega)=\rho_{L\sigma}(\omega)+\rho_{R\sigma}(\omega)$, and (ii) *antiparallel*, i.e., the magnetization direction of one of the leads (let us consider the right one) is reverted so $\rho_{R\sigma}(\omega)\to\rho_{R\bar{\sigma}}(\omega)$, where $\bar{\sigma}=\downarrow(\uparrow)$ if $\sigma=\uparrow(\downarrow)$, so the total DOS is described then by $\rho_\sigma(\omega)=\rho_{L\sigma}(\omega)+\rho_{R\bar{\sigma}}(\omega)$. Here, D_0 labels the full (generalized) bandwidth of the conduction band (further details can be found below). Effects related to leads with noncollinear leads' magnetization are not discussed here.[23]

For the special case of both leads made of the same material in the parallel alignment, $\rho_{L\sigma}(\omega)=\rho_{R\sigma}(\omega)$ and, in the antiparallel alignment, $\rho_{L\sigma}(\omega)=\rho_{R\bar{\sigma}}(\omega)$. Therefore, for the antiparallel case, it gives the total DOS to be spin independent, $\rho_\uparrow(\omega)=\rho_{L\uparrow}(\omega)+\rho_{R\downarrow}(\omega)=\rho_{L\downarrow}(\omega)+\rho_{R\uparrow}(\omega)=\rho_\downarrow(\omega)$. In a such situation, one can expect the usual Kondo effect as for normal (nonferromagnetic) metallic leads; however, the conductance will be diminished due to mismatch of the density of states described by the prefactor of the integral in Eq. (23).

B. Different band structures

In this paper, we will consider different types of total spin-dependent band structures $\rho_\sigma(\omega)$ independently of the particular magnetization direction of leads. The particular magnetization configuration will affect only the linear conductance G_σ due to the DOS mismatch for both leads, as will be discussed in detail later.

1. Flat band

The simplest situation where one can account spin asymmetry is a flat band with the energy-independent DOS $\rho_\sigma(\omega)=\rho_\sigma$. Then, the spin asymmetry can be parametrized just by a single parameter, the spin imbalance in the DOS at the Fermi energy $\omega=0$. For flat bands, the knowledge of the spin polarization P of the leads, defined as

$$P=\frac{\rho_\uparrow(0)-\rho_\downarrow(0)}{\rho_\uparrow(0)+\rho_\downarrow(0)}, \tag{5}$$

is sufficient to fully parametrize $\rho_\sigma(\omega)$ (see Fig. 2). This particular DOS shape is special due to the fact that the particle-hole symmetry is conserved in the electrodes leading to a particular behavior for the symmetric Anderson model. This type of model of the leads will be considered in Sec. V.

2. Stoner splitting

One can generalize this model and break the particle-hole symmetry by taking the Stoner splitting into account. A consequence of the conduction electron ferromagnetism is that the spin-dependent bands are shifted relative to each other (see Fig. 1). For a finite value of that shift Δ_σ, the spin-σ band is in the range $-D+\Delta_\sigma \leqslant \omega \leqslant D+\Delta_\sigma$ (with the "original" bandwidth D). In the limit $\Delta_\sigma=0$, only energies within the interval $[-D;D]$ are considered, a scheme usually used in the NRG calculations.[7] This relative shift between the two spin-dependent bands leads to the so-called Stoner splitting Δ, defined as

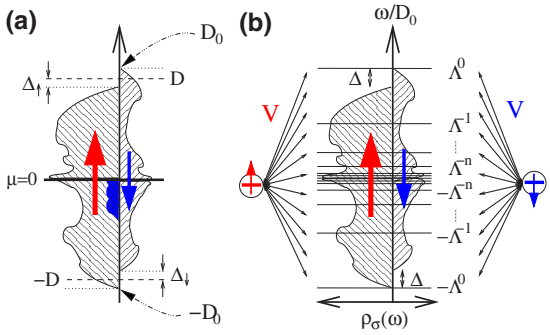

FIG. 1. (Color online) (a) Example of an energy- and spin-dependent lead DOS $\rho_\sigma(\omega)$ with an additional spin-dependent shift Δ_σ. To perform the logarithmic discretization, a generalized bandwidth D_0 is defined. Since we allow for bands with energy and spin dependence, the discretization is performed for each spin-component separately, see panel (b). Since $\hat{\mathcal{H}}_{\ell d}$ does not include spin-flip processes, an impurity electron of spin σ [circles in panel (b)] couples to lead electrons of spin σ, $\sigma=\uparrow(\downarrow)$, only. Panel (b) also illustrates that impurity electrons couple to leads' electron and hole states with arbitrary energy ω, $|\omega|\leqslant D_0$.

$$\Delta=\Delta_\downarrow-\Delta_\uparrow, \tag{6}$$

at the band edges of the conduction band (see Fig. 10). The flat band model with a Stoner splitting and consequences of the particle-hole symmetry breaking is considered in Sec. VI.

3. Arbitrary band structure

Since the spin splitting of the dot level is determined by the coupling to all occupied and unoccupied (hole) electronic states in the leads, the shape of the whole band plays an important role. Therefore, it is reasonable to consider an arbitrary DOS shape, which cannot be parametrized by a particular set of parameters as the imbalance between $\uparrow$ and $\downarrow$ electrons at the Fermi energy or a Stoner splitting (see Fig. 1). Therefore, in Sec. VII, we will consider a model with a more complex band structure and, in Sec. III, we will develop the NRG technique for an arbitrary band structure.

III. METHOD: NUMERICAL RENORMALIZATION GROUP FOR AN ARBITRARY SPIN-DEPENDENT DENSITY OF STATES

In our analysis, we take the ferromagnetic nature of the noninteracting leads by means of a spin- and energy-dependent DOS $\rho_\sigma(\omega)$ into account. A general example is given in Fig. 1. To compute the properties of the model described above, we have extended the NRG technique calculation to handle a spin-dependent density of states. In order to understand to what extent the method applied here is different from the standard NRG, it is adequate to briefly review the general concepts of NRG.

The NRG technique was invented by Wilson in the 1970s to solve the Kondo problem;[14] later, it was extended to handle other quantum impurity models as well.[24–26,28] In his original work, Wilson considered a spin-independent flat density of states for the conduction electrons. Closely fol-

lowing Refs. 17 and 27, where the mapping for the case of energy-dependent DOS was given, we generalize that procedure for the case of the Hamiltonian given in Eq. (4) which contains leads with an energy and spin-dependent DOS.

It is convenient to bring the Hamiltonian given by Eq. (4) into a continuous representation[27] before the generalized mapping is started. The replacement of the discrete fermionic operators by continuous ones, $\alpha_{k\sigma} \rightarrow \alpha_{\omega\sigma}$, translates the lead and the tunneling part of the Hamiltonian into

$$\hat{\mathcal{H}}_\ell = \sum_\sigma \int_{-1}^{1} d\omega g_\sigma(\omega) \alpha^\dagger_{\omega\sigma} \alpha_{\omega\sigma}, \tag{7}$$

$$\hat{\mathcal{H}}_{\ell d} = \sum_\sigma \int_{-1}^{1} d\omega h_\sigma(\omega) (d^\dagger_\sigma \alpha_{\omega\sigma} + \text{H.c.}). \tag{8}$$

As shown in Ref. 27, the hereby defined generalized *dispersion* $g_\sigma(\omega)$ and *hybridization* $h_\sigma(\omega)$ functions have to satisfy the relation

$$\frac{\partial g_\sigma^{-1}(\omega)}{\partial \omega} \{h_\sigma[g_\sigma^{-1}(\omega)]\}^2 = \rho_\sigma(\omega)[V_\sigma(\omega)]^2, \tag{9}$$

where $g_\sigma^{-1}(\omega)$ is the inverse of $g_\sigma(\omega)$, which ensures that the action on the impurity site is identical both in the discrete and the continuous representation. Note that there are many possibilities to satisfy Eq. (9).

The key idea of Wilson's NRG[14] is a logarithmic discretization of the conduction band, by introducing a discretization parameter Λ, which defines energy intervals $]-D_0\Lambda^{-n}; -D_0\Lambda^{-n-1}]$ and $[D_0\Lambda^{-n-1}; D_0\Lambda^{-n}[$ in the conduction band ($n \in \mathbf{N}_0$). Within the nth interval of width $d_n = \Lambda^{-n}(1-\Lambda^{-1})$, a Fourier expansion of the lead operators $\Psi^\pm_{np}(\omega)$ with fundamental frequency $\Omega_n = 2\pi/d_n$ is defined as

$$\Psi^\pm_{np}(\omega) = \begin{cases} \dfrac{1}{\sqrt{d_n}} e^{\pm i \Omega_n p \omega} & \text{if } \Lambda^{-(n+1)} \leqslant \pm\omega < \Lambda^{-n} \\ 0 & \text{otherwise.} \end{cases}$$

Here, the subscripts n and p ($\in \mathbf{Z}$) label the corresponding interval and the harmonic index, respectively, while the superscript marks positive (+) or negative (−) intervals, respectively.

The above defined Fourier series now allows one to replace the continuous fermionic conduction band operators $a_{\omega\sigma}$ by discrete ones $a_{np\sigma}$ ($b_{np\sigma}$) of harmonic index p and spin σ acting on the nth positive (negative) interval only,

$$\alpha_{\omega\sigma} = \left\{ \sum_{np} [a_{np\sigma} \Psi^+_{np}(\omega) + b_{np\sigma} \Psi^-_{np}(\omega)] \right\}. \tag{10}$$

Impurity electrons couple *only* to the $p=0$ mode of the lead operators, given that the energy-dependent generalized hybridization $h_\sigma(\omega)$ is replaced by a constant hybridization, $h_\sigma(\omega) \rightarrow h^+_{n\sigma}$ for $\omega > 0$ (or $h^-_{n\sigma}$ for $\omega < 0$, respectively). Obviously, the particular choice of constant hybridization $h^\pm_{n\sigma}$ demands the generalized dispersion $g_\sigma(\omega)$ to be adjusted accordingly, such that Eq. (9) remains valid. Details of this procedure can be found in Appendix A. Since we adopt this strategy, the harmonic index p (the impurity couples only to lead operators of harmonic index $p=0$) will be dropped below.

Defining a fermionic operator

$$f_{0\sigma} \equiv \frac{1}{\sqrt{\xi_{0\sigma}}} \sum_n (a_{n\sigma} \gamma^+_{n\sigma} + b_{n\sigma} \gamma^-_{n\sigma}), \tag{11}$$

with $\xi_{0\sigma} = \Sigma_n[(\gamma^+_{n\sigma})^2 + (\gamma^-_{n\sigma})^2] = \int_{-1}^{1} \Gamma_\sigma(\omega) d\omega$ and the coefficients $\gamma^\pm_{n\sigma}$ as given in Appendix A,[29] reveals that the impurity effectively couples to a *single* fermionic degree of freedom only, the zeroth site of the Wilson chain [for further details, see Eq. (A2)]. Therefore, the tunneling part of $\hat{\mathcal{H}}$ can be written in a compact form as

$$\hat{\mathcal{H}}_{\ell d} = \sum_\sigma \left[\sqrt{\frac{\xi_{0\sigma}}{\pi}} (d^\dagger_\sigma f_{0\sigma} + \text{H.c.}) \right]. \tag{12}$$

The final step in the NRG procedure is the transformation of the conduction band $\hat{\mathcal{H}}_\ell$ into the form of a linear chain. This goal is achieved via the tridiagonalization procedure developed by Lánczos,[30]

$$\hat{\mathcal{H}}_\ell = \sum_{\sigma n=0}^{\infty} [\varepsilon_{n\sigma} f^\dagger_{n\sigma} f_{n\sigma} + t_{n\sigma} (f^\dagger_{n\sigma} f_{n+1\sigma} + f^\dagger_{n+1\sigma} f_{n\sigma})]. \tag{13}$$

In general, the on-site energies $\varepsilon_{n\sigma}$ and hopping matrix elements $t_{n\sigma}$ along the Wilson chain need to be determined numerically. Besides the matrix elements $\epsilon_{n\sigma}$ and $t_{n\sigma}$, coefficients $u_{nm\sigma}$ and $v_{nm\sigma}$, which define the fermionic operators $f_{n\sigma}$,

$$f_{n\sigma} \equiv \sum_{m=0}^{\infty} (u_{nm\sigma} a_{m\sigma} + v_{nm\sigma} b_{m\sigma}), \tag{14}$$

already used in Eq. (13), need to be determined. One immediately anticipates the following from Eq. (11):

$$u_{0m\sigma} = \gamma^+_{m\sigma} / \sqrt{\xi_{0\sigma}}, \quad v_{0m\sigma} = \gamma^-_{m\sigma} / \sqrt{\xi_{0\sigma}}. \tag{15}$$

Equations which determine the matrix elements $\epsilon_{n\sigma}$ and $t_{n\sigma}$ and the coefficients $u_{nm\sigma}$ and $v_{nm\sigma}$ are given in Appendix B. Note that the on-site energies $\varepsilon_{n\sigma}$ vanish in the presence of particle-hole symmetry in the leads.

To summarize, Hamiltonians as the one given in Eq. (4) can be cast into the form of a linear chain $\hat{\mathcal{H}}_{\text{LC}}$,

$$\hat{\mathcal{H}}_{\text{LC}} = \hat{\mathcal{H}}_d + \sqrt{\xi_{0\sigma}/\pi} \sum_\sigma (d^\dagger_\sigma f_{0\sigma} + f^\dagger_{0\sigma} d_\sigma) + \sum_{\sigma n=0}^{\infty} [\varepsilon_{n\sigma} f^\dagger_{n\sigma} f_{n\sigma} + t_{n\sigma} (f^\dagger_{n\sigma} f_{n+1\sigma} + f^\dagger_{n+1\sigma} f_{n\sigma})], \tag{16}$$

even though one is dealing with energy- and spin-dependent leads. In general, however, this involves numerical determination of the matrix elements $\varepsilon_{n\sigma}$ and $t_{n\sigma}$,[17] in contrast to Ref. 24 (where flat bands were considered), where no closed analytical expression for those matrix elements is known.

Equation (16) nicely illustrates the strength of the NRG procedure. As a consequence of the energy separation guaranteed by the logarithmic discretization, the hopping rate

along the chain decreases as $t_n \sim \Lambda^{-n/2}$ (the on-site energies decays even faster), which allows us to diagonalize the chain Hamiltonian iteratively and, in every iteration, to keep the states with the lowest lying energy eigenvalues as the most relevant ones. This very fact underlines that this method does not rely on any assumptions concerning leading order divergences.[31]

IV. PERTURBATIVE SCALING ANALYSIS

We can understand the spin splitting of the spectral function using Haldane's scaling approach,[16] where quantum charge fluctuations are integrated out. The behavior discussed in this paper can be explained as an effect of spin-dependent quantum charge fluctuations, which lead to a spin-dependent renormalization of the dot's level position $\tilde{\epsilon}_{d\sigma}$ and a spin-dependent level broadening Γ_σ, which, in turn, induce spin splitting of the dot level and the Kondo resonance. Within this approach, a spin splitting of the local dot level, $\Delta\epsilon_d \equiv \delta\epsilon_{d\uparrow} - \delta\epsilon_{d\downarrow} + B$, which depends on the *full* band structure of the leads, is obtained[13] where

$$\delta\epsilon_{d\sigma} \simeq -\frac{1}{\pi}\int d\omega \left\{ \frac{\Gamma_\sigma(\omega)[1-f(\omega)]}{\omega - \epsilon_{d\sigma}} + \frac{\Gamma_{\bar{\sigma}}(\omega) f(\omega)}{\epsilon_{d\bar{\sigma}} + U - \omega} \right\}. \tag{17}$$

Note that the splitting is *not* only determined by the lead spin polarization P, i.e., the splitting is not only a property of the Fermi surface. Equation (17) is the key equation to explain the physics of the (spin-dependent) splitting of the local level $\epsilon_{d\sigma}$. This equation explains the spin-dependent occupation and, consequently, the splitting of the spectral function of a dot that is contacted to leads with a particular band structure. The first term in the curly brackets corresponds to electronlike processes, namely, charge fluctuations between a single occupied state $|\sigma\rangle$ and the empty $|0\rangle$ one, and the second term to holelike processes, namely, charge fluctuations between the states $|\sigma\rangle$ and $|2\rangle$. The amplitude of the charge fluctuations is proportional to Γ, which, for $\Gamma \gg T$, determines the width of dot levels observed in transport.

The exchange field given by Eq. (17) giving rise to precession of an accumulated spin on the quantum dot attached to leads with noncollinear leads' magnetization is not discussed here.[23]

A. Flat band

Equation (17) predicts that even for systems with spin asymmetric bands $\rho_\uparrow(\omega) \neq \rho_\downarrow(\omega)$, the integral can give $\Delta\epsilon = 0$, which corresponds to a situation where the renormalization of $\epsilon_{d\sigma}$ due to electronlike processes is compensated by holelike processes. An example is a system consisting of particle-hole symmetric bands, $\rho_\sigma(\omega) = \rho_\sigma(-\omega)$, where no splitting of the Kondo resonance ($\Delta\epsilon_d = 0$) for the symmetric point, $\epsilon_d = -U/2$, appears.

For a flat band, $\rho_\sigma(\omega) = \rho_\sigma$, Eq. (17) can be integrated analytically. For $D_0 \gg U$, $|\epsilon_d|$, one finds $\Delta\epsilon \simeq (P\Gamma/\pi)\mathrm{Re}[\phi(\epsilon_d) - \phi(U+\epsilon_d)]$, where $\phi(x) \equiv \Psi(\frac{1}{2} + ix/2\pi T)$ and $\Psi(x)$ denotes the digamma function. For $T = 0$, the spin splitting is given by

$$\Delta\epsilon_d \simeq \frac{P\Gamma}{\pi} \ln\left(\frac{|\epsilon_d|}{|U+\epsilon_d|} \right), \tag{18}$$

showing a logarithmic divergence for $\epsilon_d \to 0$ or $U + \epsilon_d \to 0$.

B. Stoner splitting

For real systems, particle-hole (p-h) symmetric bands cannot be assumed; however, the compensation $\Delta\epsilon = 0$ using a proper tuning of the gate voltage ϵ_d is still possible. We can also analyze the effect of the Stoner splitting by considering a flat band structure in Fig. 2 using the value of the Stoner splitting $\Delta = 0.2\left(\frac{D}{D_0}\right)D_0$. Then, also from Eq. (17), we can expect an additional spin splitting of the dot level induced by the presence of the Stoner field in the leads even for spin polarization $P = 0$ given by

$$\Delta\epsilon_d^{(\mathrm{St})} \simeq \frac{\Gamma}{2\pi} \ln\left[\frac{(-\epsilon_d + D_0 - \Delta)(U + \epsilon_d + D_0 - \Delta)}{(-\epsilon_d + D_0)(U + \epsilon_d + D_0)} \right], \tag{19}$$

which, for the symmetric level position, $\epsilon_d = -U/2$, leads to

$$\Delta\epsilon_d^{(\mathrm{St})} \simeq \frac{\Gamma}{\pi} \ln\left(\frac{U/2 + \epsilon_d + D_0 - \Delta}{U/2 + \epsilon_d + D_0} \right), \tag{20}$$

Equation (19) also shows that the characteristic energy scale of the spin splitting is given by Γ rather than by the Stoner splitting Δ ($\Delta \gg \Gamma$), since the states far from the Fermi surface enter Eq. (17) only with a logarithmic weight. The difference can be as large as 3 orders of magnitude, so, in a metallic ferromagnet, the Stoner splitting energy is of the order $\Delta \sim 1$ eV but the effective molecular field $\Delta\epsilon_d^{(\mathrm{St})}$ gen-

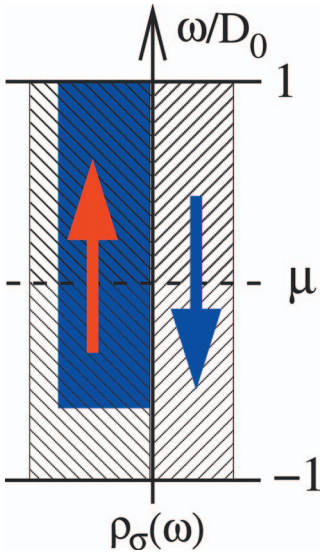

FIG. 2. (Color online) The lead density of states of a flat $[\rho_s(\omega) = \rho_\sigma]$ but spin-dependent ($\rho_\uparrow \neq \rho_\downarrow$) band for spin polarization $P = 0.2$. The dark region marks the filled states below the Fermi energy. Since $\Delta_\uparrow = \Delta_\downarrow = 0$, the generalized bandwidth $D_0 = D$.

erated by it is still a small fraction of Γ—of order of 1 meV, comparable with the Kondo energy scale for molecular single-electron transistors.[10] However, the Stoner splitting introduces a strong p-h asymmetry, so it can influence the character of the gate voltage dependence significantly.

In the next section, we analyze the effect of different types of the band structure using numerical renormalization group technique and compare it to that obtained in this section by scaling procedure.

V. FLAT BANDS WITHOUT STONER SPLITTING

We start our analysis by considering normalized flat bands without the Stoner splitting (i.e., $D_0=D$), as sketched in Fig. 2, with finite spin polarization $P\neq 0$ [defined via Eq. (5)].[32] In this particular case of spin (but not energy) dependent coupling, $\Gamma_\sigma \equiv \pi\rho_\sigma V^2$, the coupling Γ_σ can be parametrized via P, $\Gamma_{\uparrow(\downarrow)}=\frac{1}{2}\Gamma(1\pm P)$ [here, + (−) corresponds to spin ↑ (↓)], where $\Gamma=\Gamma_\uparrow+\Gamma_\downarrow$. Leads with a DOS as the one analyzed in this section have, for instance been studied in Refs. 7 and 8.

Since $\Gamma_\sigma \equiv \pi\rho_\sigma V^2$, the spin dependence of Γ_σ can be absorbed by replacing $V\rightarrow V_\sigma=V\sqrt{\frac{1}{2}(1\pm P)}$ in Eq. (4), i.e., a spin-dependent *hopping* matrix element, while treating the leads as unpolarized ones ($\rho_\sigma\rightarrow\rho$). This procedure has the particular advantage that the "standard" NRG procedure[24] can be applied, meaning that the on-site energies (tunneling matrix elements) [defined in Eq. (13)] along the Wilson chain $\varepsilon_{n\sigma}$ vanish, while $t_{n\sigma}$ turn out to be spin *independent*. Therefore, it does not involve the solution of the tedious equations given in Appendix B.

A. Spin and charge state

Consequently, we start our numerical analysis by computing the spin-resolved dot occupation $n_\sigma \equiv \langle \bar{n}_\sigma \rangle$, which is a static property. Figure 3 shows the spin resolved impurity occupation as a function of the spin polarization P of the leads. Figure 3(a) and 3(c) correspond to a gate voltage of $\epsilon_d=-U/3$ (where the total occupation of the system $n_\uparrow+n_\downarrow<1$) whereas the second line corresponds to $\epsilon_d=-2U/3$ (with $n_\uparrow+n_\downarrow>1$). The total occupation of the system, $n_\uparrow+n_\downarrow$, decreases (increases) for $\epsilon_d=-U/3$ ($\epsilon_d=-2U/3$) when the spin polarization of the leads is finite, $P\neq 0$. Note that both situations, $\epsilon_d=-U/3$ and $\epsilon_d=-2U/3$, are symmetric with respect to changing particle into hole states and vice versa, which is possible only for the leads with particle-hole symmetry. For the gate voltage $\epsilon_d=-U/2$, there is a particle-hole symmetry in the whole system leads with a DOS which does share this symmetry even in the presence of spin asymmetry. Note that whereas a finite spin polarization leads to a decrease in $n_\uparrow+n_\downarrow$ for $\epsilon_d>-U/2$ [see Fig. 3(a)], it results in an increase in $n_\uparrow+n_\downarrow$ for $\epsilon_d<-U/2$ [see Fig. 3(b)]. Obviously, for $P=0$ and in the absence of an external magnetic field, the impurity does not have a preferred occupation, $n_\uparrow=n_\downarrow$. Any finite value of P violates this relation: $n_\uparrow>n_\downarrow$ for $P>0$ and $\epsilon_d>-U/2$ (since $\delta\epsilon_{d\uparrow}\sim\Gamma_\downarrow<\Gamma_\uparrow\sim\delta\epsilon_{d\downarrow}$). For $\epsilon_d<-U/2$, on the other hand, the opposite behavior is found.

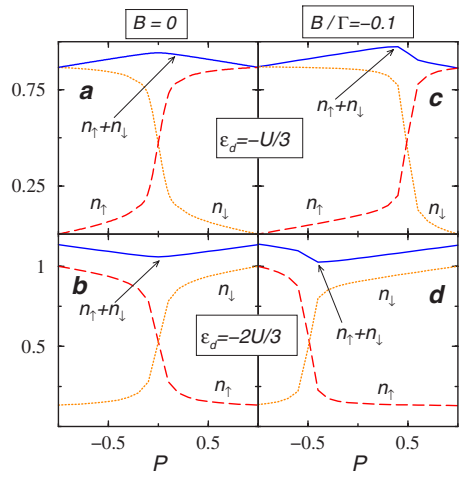

FIG. 3. (Color online) [(a)–(d)] Spin-dependent occupation n_σ of the local level as a function of the leads' spin polarization P for $\epsilon_d=-U/3$ [(a) and (c)] and $\epsilon_d=-2U/3$ [(b) and (d)] (related by the particle-hole symmetry) for $B=0$ (left column) and $B=-0.1\Gamma$ (right column). For finite spin-polarization, $P\neq 0$, the condition $n_\uparrow=n_\downarrow$ can only be obtained by an appropriately tuned magnetic field, as shown in (c) and (d). Parameters: $U=0.12D_0$ and $\Gamma=U/6$.

The effect on the impurity of a finite lead polarization, namely, to prefer a certain spin species, can be compensated by a locally applied magnetic field, as shown in Figs. 3(c) and 3(d). For $\epsilon=-U/3$ and $B/\Gamma=-0.1$ [see Fig. 3(c)], the impurity is *not* occupied by a preferred spin species, $n_\uparrow=n_\downarrow$, for $P\sim 0.5$. Due to particle-hole symmetry, the same magnetic field absorbs a lead polarization of $P\sim -0.5$ for $\epsilon=-2U/3$ [see Fig. 3(d)]. The magnetic field which restores the condition $n_\uparrow=n_\downarrow$, henceforth denoted as compensation field $B_{\mathrm{comp}}(P)$, will be of particular interest below.

B. Single-particle spectral function

Using the NRG technique we can access the spin-resolved single-particle spectral density $A_\sigma(\omega,T,B,P)=-\frac{1}{\pi}\,\mathrm{Im}\,\mathcal{G}^R_{d,\sigma}(\omega)$ for arbitrary temperature T, magnetic field B, and spin polarization P, where $G^R_\sigma(\omega)$ denotes a retarded Green function. We can relate the asymmetry in the occupancy, $n_\uparrow\neq n_\downarrow$, to the occurrence of charge fluctuations in the dot and broadening and shifts of the position of the energy levels (for both spins up and down). For $P\neq 0$, the charge fluctuations, and hence level shifts and level occupations, become spin dependent, causing the dot level to split[6] and the dot magnetization $n_\uparrow-n_\downarrow$ to be finite. As a result, the Kondo resonance is also spin split and suppressed [Fig. 4(b)], similarly to the effect of an applied magnetic field.[33] This means that Kondo correlations are reduced or even completely suppressed in the presence of ferromagnetic leads.

Note the asymmetry in the spectral function for $P\neq 0$ which stems from the spin-dependent hybridization Γ_σ. Figure 4(b), where the spin-resolved spectral function is plotted, reveals the origin of the asymmetry around the Fermi energy of the spectral function. The spectral function obtained for polarized leads has to be contrasted to that of a dot asserted

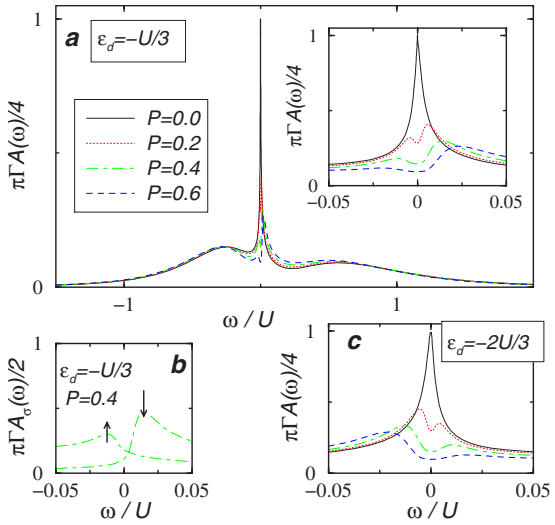

FIG. 4. (Color online) Total spectral functions $A(\omega)=\Sigma_\sigma A_\sigma(\omega)$ for various values of the spin polarization P. (a) For $\epsilon_d=-U/3$, an increase in P results in a splitting and suppression of the Kondo resonance (see inset). The effect of finite P on the Hubbard peaks is less significant. The spin-resolved spectral function $A_\sigma(\omega)$, shown in (b), reveals that $A_\uparrow(\omega)$ and $A_\downarrow(\omega)$ differ significantly from each other for $P\neq 0$. (c) Spectral function for the same values of P as in (a) but for $\epsilon_d=-2/3U$ [due to particle-hole symmetry, the results are mirrored as compared to (a) but with inverted spins]. Parameters: $U=0.12D_0$, $B=0$, and $\Gamma=U/6$.

to a local magnetic field, where a nearly *symmetric* (perfect symmetry is only for the symmetric Anderson model) suppression and splitting of the Kondo resonance (around the Fermi energy) appear.[33] In Fig. 4(c), the gate voltage ($\epsilon_d=-2U/3$) is chosen such that it is particle-hole symmetric to the case shown in Fig. 4(a). Due to the opposite particle-hole symmetry, the obtained spectral function in Fig. 4(c) is nothing else but the spectral function shown in Fig. 4(a) mirrored around the Fermi energy.

Figures 3(c) and 3(d) showed that a finite magnetic field B can be used to recover the condition $n_\uparrow=n_\downarrow$. Indeed, for any lead polarization P, a *compensation* field $B_{\rm comp}(P)$ exists at which the impurity is not preferably occupied by a particular spin species. To a good approximation, $B_{\rm comp}(P)$ has to be chosen such that the induced spin splitting of the local level is compensated.[36,37] One consequently expects a linear P dependence of $B_{\rm comp}$ from Eq. (18). Figure 5(a) shows the P dependence of $B_{\rm comp}$ for various values of ϵ_d obtained via NRG. The numerically found behavior can be explained through Eq. (18). It confirms that the slope of $B_{\rm comp}$ is negative (positive) for $\epsilon_d>-U/2$ ($\epsilon_d<-U/2$) and that $B_{\rm comp}(P)=0$ for $\epsilon_d=-U/2$.

The fact that this occurs simultaneously with the disappearance of the Kondo resonance splitting suggests that the local spin is fully screened at $B_{\rm comp}$. The expectation of an unsplit Kondo resonance in the presence of the magnetic field $B_{\rm comp}$ is nicely confirmed by our numerics in Fig. 5(b) for $\epsilon_d=-U/3$. Moreover, the sharpening of the Kondo resonance in the spectral function upon increasing P (indicating a decrease in the Kondo temperature T_K) can be extracted from this plot. The associated binding energy of the singlet (the

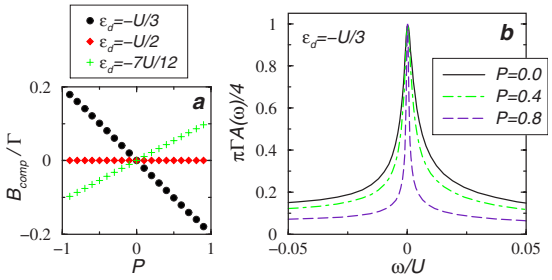

FIG. 5. (Color online) (a) Compensation field $B_{\rm comp}(P)$ for different values of ϵ_d. For flat bands, $B_{\rm comp}$ depends linearly on the lead polarization. At the point where there is particle-hole symmetry, so for gate voltage ($\epsilon_d=-U/2$), $B_{\rm comp}(P)=0$ for any value of P, i.e., the spectral function is not split for any value of P even though $B=0$. (b) Spectral function for various values of P for $B=B_{\rm comp}$. Note the sharper resonance in the spectral function, i.e., a reduced Kondo temperature T_K.

Kondo temperature T_K) is consequently reduced.

Having demonstrated that the Kondo resonance can be fully recovered for $B_{\rm comp}$ even though $P\neq 0$, we show that there is also the possibility to recover the unsplit Kondo resonance via an appropriately tuned gate voltage. In Fig. 6, we plot the spin-resolved spectral function for various values of ϵ_d for $P=0.2$ and $B=0$. Note that one can easily identify whether the Kondo resonance is fully recovered from the positions of $A_\sigma(\omega)$ relative to each other. Since a dip in the total spectral function $A(\omega)=\Sigma_\sigma A_\sigma(\omega)$ is not present for a modest shift of $A_\sigma(\omega)$ with respect to each other, we identify an unsplit Kondo resonance with perfectly aligned spin-resolved spectral functions henceforth.

Clearly, one can identify from Fig. 6 that the spectral function is split for any value $\epsilon_d\neq -U/2$. This splitting changes its sign at $\epsilon_d=-U/2$. For the particular case $\epsilon_d=-U/2$ [see Fig. 6(b)], the spectral function reaches the uni-

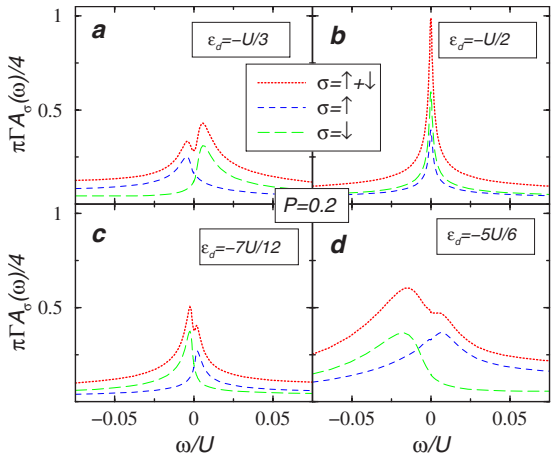

FIG. 6. (Color online) Spin-dependent spectral function $A_\sigma(\omega)$ for various values of ϵ_d, fixed $P=0.2$, and $B=0$ [(blue) dashed: $A_\uparrow(\omega)$; (green) long dashed: $A_\uparrow(\omega)$; (red) dotted: $A(\omega)=\Sigma_\sigma A_\sigma(\omega)$]. The splitting between $A_\uparrow$ and $A_\downarrow$ changes its sign at $\epsilon_d=-U/2$. The spectral function $A(\omega)$ is plotted for several values of P for $\epsilon_d=-U/3$ in Fig. 4(a). The splitting of the spectral function $A(\omega)$ depends on P as well on ϵ_d. Parameters: $U=0.12D_0$ and $\Gamma=U/6$.

tary limit. For this gate voltage, the spin-resolved spectral functions $A_\sigma(\omega)$ have a different height, as predicted from the Friedel sum rule [Eq. (21)].

C. Friedel sum rule

A direct consequence of the spin splitting of the local level and the accompaning $n_\uparrow \neq n_\downarrow$ for $P \neq 0$ and $B=0$ can be explained by means of the Friedel sum rule,[34] an exact $T=0$ relation valid also for arbitrary values of P and B. This formula relates the height of the spectral function (at the Fermi energy) and the phase shift of the electrons scattered by the impurity. As already pointed out, spin-polarized electrodes induce a splitting, the local impurity level resulting in a spin-dependent occupation of the impurity. Thus, the knowledge of the local occupation can be used to anticipate (via the Friedel sum rule) that the local spectral function becomes spin split and suppressed (similar to the presence of a local magnetic field) in the presence of spin-polarized leads.

According to the Friedel sum rule, the height of the spectral function at the Fermi energy $A_\sigma(0)$ is fully determined by the level occupation n_σ,

$$\phi_\sigma = \pi n_\sigma, \quad A_\sigma(0) = \frac{\sin^2(\pi n_\sigma)}{\pi \Gamma_\sigma}, \tag{21}$$

where ϕ_σ is the spin-dependent phase shift. This implies a split and suppressed Kondo resonance for $P \neq 0$ in the absence of a magnetic field.

An equal spin occupation, $n_\uparrow = n_\downarrow$, can be obtained only for an appropriate external magnetic field $B=B_{\text{comp}}$. For the latter, in the local moment regime ($n \approx 1$), we have $n_\uparrow = n_\downarrow \approx 0.5$, so that $\phi_\uparrow = \phi_\downarrow \approx \pi/2$, which implies that the peaks of $A_\uparrow$ and $A_\downarrow$ are aligned. Thus, the Friedel sum rule clarifies why the magnetic field B_{comp} at which the splitting of the Kondo resonance disappears coincides with that for which $n_\uparrow = n_\downarrow$. Equation (21) indicates a new feature, namely, that the amplitude of the Kondo resonance becomes spin dependent (see also the discussion in Sec. V E).

It is important to point out that Eq. (21) is valid only for the leads with particle-hole symmetry (see Ref. 35). For an arbitrary DOS shape, it is possible to generalize the Friedel sum rule.

D. Spin-spectral function: Kondo temperature

We already stated above that the Kondo temperature T_K decreases when the lead polarization P is increased. Obviously, T_K has to vanish when we are dealing with fully spin-polarized leads, $|P|=1$. To obtain $T_K(P)$, we calculated the imaginary part of the quantum dot spin spectral function,

$$\chi_S^z(\omega) = \mathcal{F}\{i\Theta(t)\langle[S_z(t), S_z(0)]\rangle\} \tag{22}$$

($\mathcal{F}$ denotes the Fourier transform) [see also Fig. 7(a)], in the presence of the appropriate $B_{\text{comp}}(P, \epsilon_d)$ and identified the maximum in Im χ_S^z with $T_K(P)$. Figure 8(a) shows $T_K(P)$ normalized to $T_K(P=0)$ for different values of ϵ_d. As shown in Refs. 6 and 7, the functional dependence of $T_K(P)$ can be

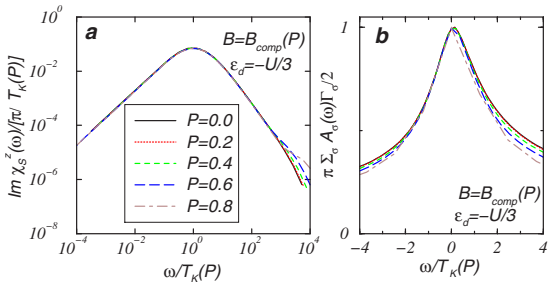

FIG. 7. (Color online) The isotropic Kondo effect, accompanied by universal scaling, can be recovered even for $P \neq 0$ and $B = B_{\text{comp}}$ since both (a) the spin-susceptibility Im χ_S^z and (b) the spectral function collapse onto a universal curve. This statement holds for any value of ϵ_d with some corresponding compensation fields, as given in Fig. 5(a). Parameters: $U=0.12D_0$, $\epsilon_d=-U/3$, and $\Gamma = U/6$.

nicely explained within the framework of a poor man's scaling. Note that the decrease in T_K is rather weak for a modest value of P. In Fig. 7(b), we plot, in addition to $T_K(P)$, the gate voltage dependence of $T_K(\epsilon_d)$ normalized to $T_K(\epsilon_d = -U/2)$ (where the Kondo temperature is minimal) for fixed $P=0.2$. In the presence of $B_{\text{comp}}(P, \epsilon_d)$, this functional dependence of the Kondo temperature can be analytically described via Haldane's formula[16] for the Kondo temperature of a single-level dot coupled to unpolarized leads, $T_K = \frac{1}{2}\sqrt{U\Gamma}e^{\pi\epsilon_d(\epsilon_d+U)/\Gamma U}$. This fact is another manifestation that indeed the usual Kondo effect can be recovered in the presence of spin-polarized leads, given that the appropriate $B_{\text{comp}}(P, \epsilon_d)$ is applied.

Having shown that the coexistence of spin polarization in the leads and the Kondo effect is possible (given that a magnetic field B is tuned appropriately at a given gate voltage ϵ_d), we plot the properly rescaled spin susceptibility Im χ_S^z [see Fig. 7(a)], and the spectral function [see Fig. 7(b)], confirming that the isotropic Kondo effect is recovered. The expected collapse of Im χ_S^z and $\Sigma_\sigma \Gamma_\sigma A_\sigma(\omega)$ onto a universal

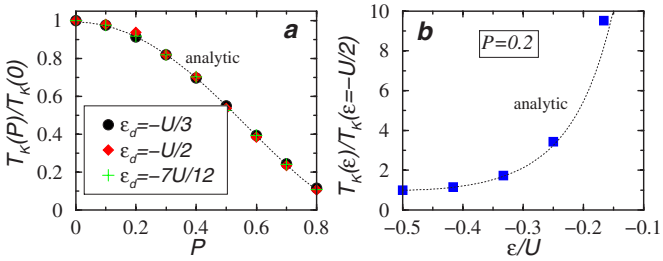

FIG. 8. (Color online) (a) Spin polarization dependence of the Kondo temperature $T_K(P)$ [obtained by applying an appropriate $B = B_{\text{comp}}(P, \epsilon_d)$]. The functional dependence of $T_K(P)$ found via a poor man's scaling analysis (dotted line) [see Eq. (6) of Ref. 6] is confirmed by the NRG analysis. The plot confirms that a dot tuned to the local moment regime, $\Sigma_\sigma n_\sigma \simeq 1$, shows the universal P dependence of $T_K(P)$ for arbitrary values of ϵ_d. (b) The ϵ_d dependence of T_K for fixed $P=0.2$ at $B=B_{\text{comp}}$. As long as the impurity remains in the local moment regime, Haldane's formula (Ref. 16) for T_K (dotted line) properly describes $T_K(\epsilon_d)$ even though the leads have a finite spin polarization. Parameters: $U=0.12D_0$ and $\Gamma = U/6$.

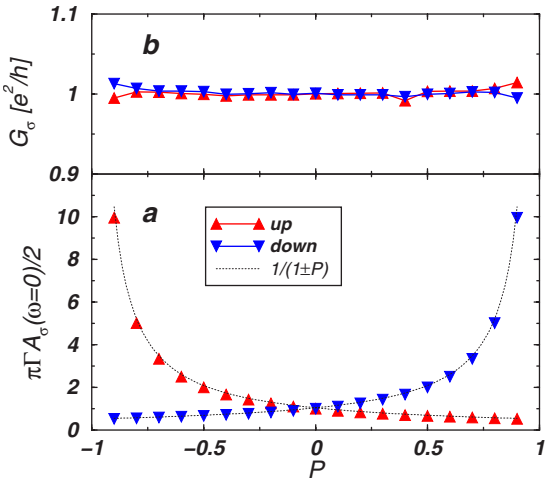

FIG. 9. (Color online) (a) Height of the spin-resolved spectral function $A_\sigma(\omega=0)$ as a function of P. The dashed line shows the $1/(1\pm P)$ dependence as expected from the Friedel sum rule [Eq. (21)]. (b) Spin-resolved conductance G_σ as obtained from Eq. (23). This plot confirms the expectation based on the Friedel sum rule that the spin-resolved conductance should be independent of the spin species, consequently, it serves as a consistency check of our numerics.

curve for temperatures below T_K [note that T_K depends on P, see, e.g., Fig. 5(b)] is confirmed by our numerical results. For energies much bigger than T_K, $\omega \gg T_K$, universal scaling is lost and the curves start to deviate from each other.

E. Conductance

The knowledge of the spectral function enables us to compute quantities which are experimentally accessible, such as the linear conductance. To investigate the question whether spin-polarized ferromagnetic leads introduce a spin-dependent current, we compute the spin-resolved conductance G_σ,

$$G_\sigma = \frac{e^2}{\hbar}\frac{2\Gamma_{L\sigma}\Gamma_{R\sigma}}{(\Gamma_{L\sigma}+\Gamma_{R\sigma})}\int_{-\infty}^{\infty} d\omega A_\sigma(\omega)\left[-\frac{\partial f(\omega)}{\partial \omega}\right], \quad (23)$$

with $f(\omega)$ denoting the Fermi function (remember that we choose $\Gamma_{L\sigma}=\Gamma_{R\sigma}$). The total conductance G is nothing else but the sum of the spin-resolved conductances $G=\Sigma_\sigma G_\sigma$. Based on the Friedel sum rule [Eq. (21)], we expect the height of the spin-resolved spectral function at the Fermi energy $A_\sigma(0)\sim 1/\Gamma_\sigma \sim 1/(1\pm P)$. This expectation is nicely confirmed by our numerical results in Fig. 9(a). As the $T=0$ conductance is given by the product of $A_\sigma(0)$ and Γ_σ, the spin-resolved conductance $G_\sigma \sim \Gamma_\sigma A_\sigma(0)$ becomes P independent. The results of the NRG calculation are shown in Fig. 9(b), confirming this expectation. We conclude that, even though one is dealing with spin-polarized leads, it is *not* possible to create a spin current via spin-polarized leads; the current remains spin independent. For the antiparallel alignment due to the DOS mismatch, the conductance will be reduced below the $G_0=2e^2/h$ limit.

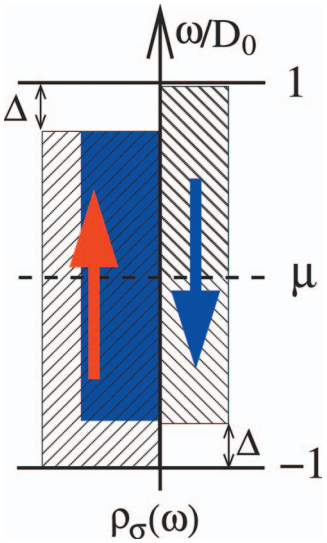

FIG. 10. (Color online) The DOS in the case of flat bands with the Stoner splitting Δ and a finite spin polarization P. In general, the shifts of the $\uparrow$ and $\downarrow$ bands are unrelated to each other, $\Delta_\downarrow \neq -\Delta_\uparrow$. In this section, however, we assume $\Delta_\downarrow=-\Delta_\uparrow$.

VI. FLAT BANDS WITH STONER SPLITTING

In ferromagnetic leads, in addition to a finite lead spin polarization P at the Fermi surface, a splitting between the spin-$\uparrow$ and spin-$\downarrow$ bands, Δ_σ (Stoner splitting), which is an effect of the effective exchange magnetic field in the leads, might appear. Taking this effect into account we do *not* expect the splitting of the Kondo resonance to disappear at $\epsilon_d=-U/2$, as in Fig. 6(b), rather at a different value of ϵ_d determined by the shifts Δ_σ. This is due to the fact that the Stoner splitting breaks the particle-hole symmetry in the electrodes. Consequently, we shall consider flat, spin-polarized leads (of polarization P), which are shifted relative to each other by an amount Δ_σ in this section. Since particle-hole symmetry is lost for this band structure, in the leads, we expect neither the splitting of the Kondo resonance, see, e.g., Fig. 6, nor the compensation field B_{comp} to be symmetric around $\epsilon_d=-U/2$, in contrast to Sec. V.

To quantify the statement that a shift Δ_σ introduces a finite exchange field and splitting, in this section we analyze the particular case $\Delta_\downarrow=-\Delta_\uparrow=\Delta$, sketched in Fig. . Note that the lead DOS structure discussed in this section[38] already requires the use of the extended NRG scheme, explained in Sec III. In particular, spin-dependent on-site energies along the Wilson chain $\epsilon_{n\sigma}$, as explained in Sec. III and Appendixes A and B, need to be determined to solve for the lead band structure shown in Fig. 10.

The studies summarized in Sec. V revealed that the spin-resolved impurity occupation n_σ is the key quantity in the context of a dot contacted to spin-polarized leads. Following this finding, we plot n_σ vs P for leads with $\Delta=0.1\left(\frac{D}{D_0}\right)D_0$ and $\epsilon_d=-U/3$ in Fig. 11. In contrast to the previous section, the impurity is preferably occupied by $\downarrow$ electrons in the absence of a magnetic field [see Fig. 11(a)] even for $P=0$. A finite magnetic field, e.g., $B/\Gamma=0.1$ [Fig. 11(b)], has the same con-

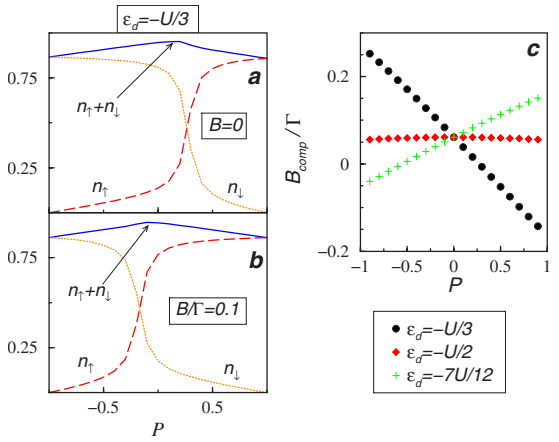

FIG. 11. (Color online) Spin polarization P dependence of the local occupation n_σ for (a) $B=0$ and (b) $B=0.1\Gamma$ with $\epsilon_d=-U/3$. The Stoner splitting Δ even in the absence of spin polarization of the leads, $P=0$, introduces an effective exchange field which splits the local level $n_\downarrow > n_\uparrow$ in the absence of an external magnetic field $B=0$. The spin polarization dependence of B_{comp} for various values of ϵ_d is shown in (c). To a good approximation, the Stoner splitting introduces a constant exchange field (here, $B_{\mathrm{comp}}/\Gamma \approx 0.061$); therefore, it does nothing else but shift the B_{comp} dependence of Sec. V. Parameters: $U=0.12\left(\frac{D}{D_0}\right)D_0$, $\Gamma=U/6$, and $\Delta_\downarrow=-\Delta_\uparrow=0.10\left(\frac{D}{D_0}\right)D_0$.

sequence as described before, namely, the shift of the local impurity levels $\epsilon_{d\sigma}$. The P dependence of B_{comp} for the particular band structure sketched in Fig. 10 is shown in Fig. 11(c); it is roughly given by the compensation field for flat bands [Fig. 5(a)], where the same gate voltages were used, shifted by an effective exchange field $\Delta\epsilon_d^{(\mathrm{St})}$ generated by the band splittings for $P=0$. The value of B_{Stoner} can be obtained via integrating out those band states of energy ω which lie in the interval $D \leqslant |\omega| \leqslant D_0$ [see Eq. (20)]. The value of this effective exchange field, which is logarithmically suppressed (as can be shown by perturbative scaling) is given by Eq. (20). Inserting the numbers used in this section, we obtain a $\Delta\epsilon_d^{(\mathrm{St})}/\Gamma \approx 0.060$. The numerical calculation reveals $\Delta\epsilon_d^{(\mathrm{St})}/\Gamma \approx 0.061$ [see Fig. 11(c)], i.e., the numerical result agrees reasonably well with the result based on the scaling analysis (see Sec. IV).

Finite temperature: Comparison with experimental data

In a recent experiment of Nygård *et al.*[11] an anomalous splitting of the zero bias anomaly in the conductance induced by the Kondo resonance in the *absence* of a magnetic field was observed. In this experiment, quantum dot based on single wall carbon nanotubes contacted to nonmagnetic, spin unpolarized Cr/Au electrodes were used. Those authors related the observed splitting of the Kondo resonance at zero magnetic field with the presence of a ferric iron nitrate nanoparticle,[39] which, due to electronic tunnel coupling to the dot, introduces a spin-dependent hybridization.

We model the setup of Ref. 11 by means of a single-level dot tuned to the local moment regime $\epsilon_{d\sigma}=-U/2$ [dashed line in Fig. 1(b) of Ref. 11]. Moreover, we used $T_K=500$ mK,[40] which is roughly the value of T_K observed in

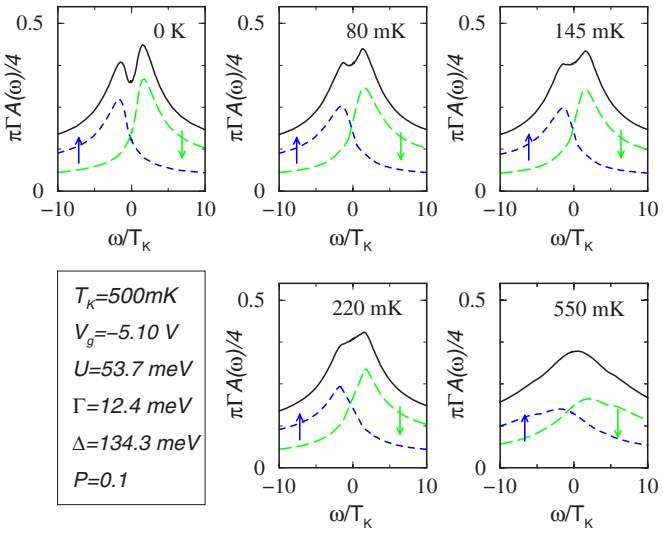

FIG. 12. (Color online) Spin-resolved equilibrium spectral function $A_\sigma(\omega,T,V=0)$ with parameters extracted from Ref. 11. The (blue) dashed lines correspond to $A_\uparrow(\omega,T,V=0)$, the (green) long dashed lines to $A_\downarrow(\omega,T,V=0)$, and the (red) solid ones to the sum of both, i.e., $A(\omega,T,V=0)$. [(a)–(e)] A gradual increase in the temperature for those temperatures used in Ref. 11. For comparison, we plot the $T=0$ spectral function $A(\omega,T=0,V=0)$ in panel (a) as well. Note that the splitting of the Kondo resonance disappears upon increasing T.

Ref. 11, as an input parameter and extracted $U/\Gamma=4.3$ from this value. Since a splitting of the Kondo resonance was observed for $\epsilon_{d\sigma}=-U/2$, see, e.g., Fig. 1(b) of Ref. 11, a particle-hole asymmetry must exist to achieve a splitting. We try to model this effect by a using flat band structure and by introducing the Stoner splitting. We find the best agreement between the experimentally observed splitting of the Kondo resonance for $\Delta/U=2.5$. The presence of the nanoparticle introduces a spin-dependent hybridization which we parametrize via the lead spin polarization P.

The comparison of the dI/dV vs V characteristics of Ref. 11 with the theoretical result turns out to be rather complicated as it involves the *nonequilibrium* spectral function $A(\omega,T,V)$ which itself is not known how to compute accurately.[41,42] It is possible to compare qualitatively the splitting in the nonequilibrium conductance obtained in the experiment to the single-particle spectral function. Due to the splitting in the particle spectral function for the dot, which is strongly related to the low-bias conductance measurements, we find close similarity between both of them. When we approximate the experimental results of dI/dV with $A(\omega,T,V=0)$, we achieve the best agreement between theory and experiment for $P=0.1$. For these parameters ($\epsilon_{d\sigma}=-U/2$, $U/\Gamma=4.3$, $\Delta/U=2.5$, and $P=0.1$), we compute the temperature-dependent equilibrium spectral function $A(\omega,T,V=0)$ presented in Fig. 12.

The numerical findings shown in Fig. 12 qualitatively confirm the behavior found in the experiment of Nygård *et al.*, namely, vanishing splitting in the dI/dV curves with increasing temperature. In the experiment, however, the differential conductance dI/dV turns out to be asymmetric around

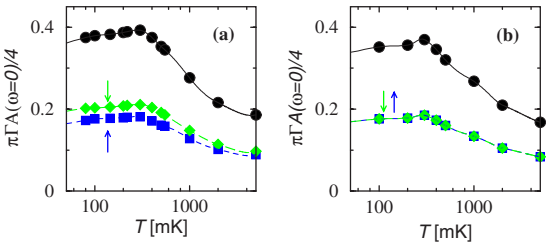

FIG. 13. (Color online) Linear conductance as a function of temperature (a) for the model studied in this section and (b) for the case of a dot coupled to normal spin unpolarized leads ($P=0$ and $\Delta=0$) but in the presence of a magnetic field $B=0.02U$. In both cases, a plateau in the linear conductance around T_K can be observed. Whereas the spin-resolved linear conductance is degenerate in case (b) (since it is the symmetric Anderson model with particle-hole symmetry), this is not the case for (a). Parameters are as in Fig. 12 except for $P=\Delta=0$ in case (b).

the Fermi energy [see Figs. 2(b)–2(d) in Ref. 11]. We attribute the asymmetry in the dI/dV curve to the asymmetry in the coupling between left and right leads.

Finally, we want to compare the temperature dependence of the linear conductance G found in Ref. 11 [see Fig. 2(a) of Ref. 11] with the one based on the model described above. In the absence of a magnetic field $B=0$ and source-drain voltage $V=0$, a plateau in G was found around $T\approx 500$ mK in the experiment. Note that the calculation of G does not involve the nonequilibrium spectral function so we can calculate it exactly. In Fig. 13(a), we show the theoretical curve of the spin-resolved conductance G_σ obtained via Eq. (23) for the model discussed in this section. In agreement with the experiment, a plateau in the linear conductance G is found around T_K.

For comparison, we also plot the linear conductance of a dot contacted to normal spin-unpolarized leads (i.e., flat-bands with $P=0$ which are not shifted relative to each other) for increasing temperature but in the *presence* of a finite magnetic field $B=0.02U$ in Fig. 13(b). Such a magnetic field might, e.g., be inserted in to the system via the presence of the ferromagnetic nanoparticles. Also, such a scenario leads to a plateau in G. The value of the associated magnetic field, however, is rather big, $B=0.02U$, corresponding to $B\approx 1$ T [here, we assumed $g=2.0$ for the conduction electrons in the nanotube (see also Ref. 11)]. According to Ref. 11, the latter scenario can therefore *not* explain the observed behavior, since one can argue that such a large magnetic field can hardly be believed to exist in this experiment (see, in particular, footnote 13 of Ref. 11).

Consequently, the presence of ferromagnetic leads might explain the experimental observation. We can, however, not exclude other possible mechanisms—such as the existence of an effective magnetic field—which might lead to the observed behavior but, only from special geometry, where the strong stray magnetic field is possible.

VII. BAND STRUCTURE WITH ARBITRARY SHAPE

Flat bands, studied in the previous sections, are only a poor approximation of a realistic band structure in the leads.[43] We complete our study by analyzing the effect of an *arbitrary* lead DOS. Consequently we are considering leads with a DOS which is energy and spin dependent and additionally contains a Stoner splitting in this section. As outlined in the previous section, the "generalized" NRG formalism introduced in Sec. III has to be used in this case as well. In particular, we study the effect of gate voltage variation on the spin splitting of the local level of a quantum dot attached to ferromagnetic leads. We show how the gate voltage can control the magnetic properties of the dot. A similar proposal, namely, to control the magnetic interactions via an electric field, was recently made in gated structures.[44]

In an analysis of several types of band structures, we found three typical gate voltage dependences of the Kondo resonance. To be more specific, to illustrate this behavior, we used a square-root shape DOS or parabolic band (as for free s-type electrons)[45] with the Stoner splitting Δ (Ref. 46) and some additional spin asymmetry Q,

$$\rho_\sigma(\omega)=\frac{1}{2}\frac{3\sqrt{2}}{8}D^{-3/2}(1+\sigma Q)\sqrt{\omega+D+\sigma\Delta/2}, \qquad (24)$$

depicted in Fig. 14 [$\sigma\equiv 1(-1)$ for $\uparrow(\downarrow)$]. This example turns out to encompass three typical classes mentioned above. Note that we restricted the DOS in Eq. (24) $\omega\in[-D-\sigma\Delta/2, D-\sigma\Delta/2]$ to ensure that we are dealing with a normalized DOS.

The three typical gate voltage dependences of the Kondo resonance we found are (i) a scenario where the splitting of the local level was roughly independent of gate voltage [Fig. 15(a)], (ii) a scenario with a strong gate voltage dependence of the splitting but without compensation [Fig. 15(b)], and (iii) a case with a strong gate voltage dependence of the splitting including a particular gate voltage where the splitting vanishes [Fig. 15(c)]. Figures 16(a)–16(c) show the effect of an external magnetic field for Figs. 15(a)–15(c), respectively. As already outlined in the previous sections, an external magnetic field can be used to compensate the lead induced spin splitting (which itself depends on gate voltage) and thereby change that gate voltage where the full Kondo resonance exists [see Figs. 15(c) and 16(c)].

The spitting of the spectral function (see Figs. 15 and 16) agrees very well with the splitting based on Haldane's scaling approach[16] given by Eq. (17). The white dashed line in Figs. 15 and 16 shows prediction of Eq. (17), which fits very well to the numerical results presented.

In Figs. 17(a)–17(c), we plot the linear conductance[47] G for the three band structures sketched in Fig. 14 as a function of gate voltage ϵ_d and external magnetic field B. The two horizontal maxima in the conductance around $\epsilon_d\approx 0$ and $\epsilon_d\approx -U$ correspond to standard Coulomb resonances. The increased conductance in between, however, is due to the Kondo effect. Note that, in contrast to the Kondo effect observed in the case of a dot attached to flat and unpolarized leads (where the Kondo resonance is a vertical line), the Kondo resonance has a finite slope here. This is due to the gate voltage dependence (and, correspondingly, to the compensation field dependence) of the the spin splitting of the local level [Eq. (17)].

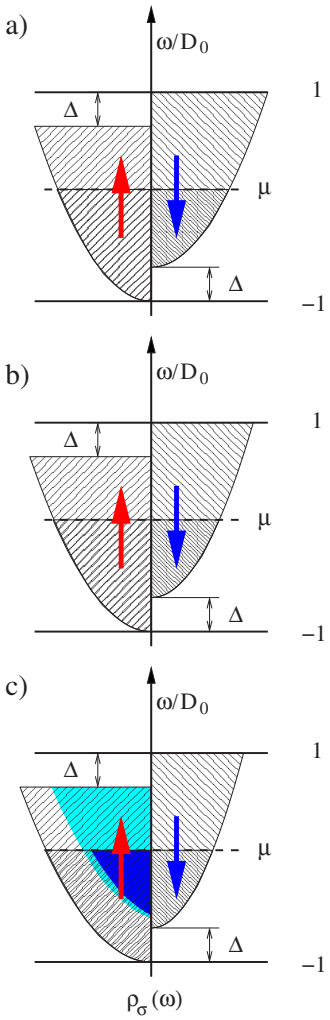

FIG. 14. (Color online) The parabolic density of states (typical for *s* electron band) given by Eq. (24) with the same Stoner splitting $\Delta=0.3D$ but with an additional spin asymmetry Q defined in the text. Here, Q=(a) 0.0, (b) 0.1, and (c) 0.3.

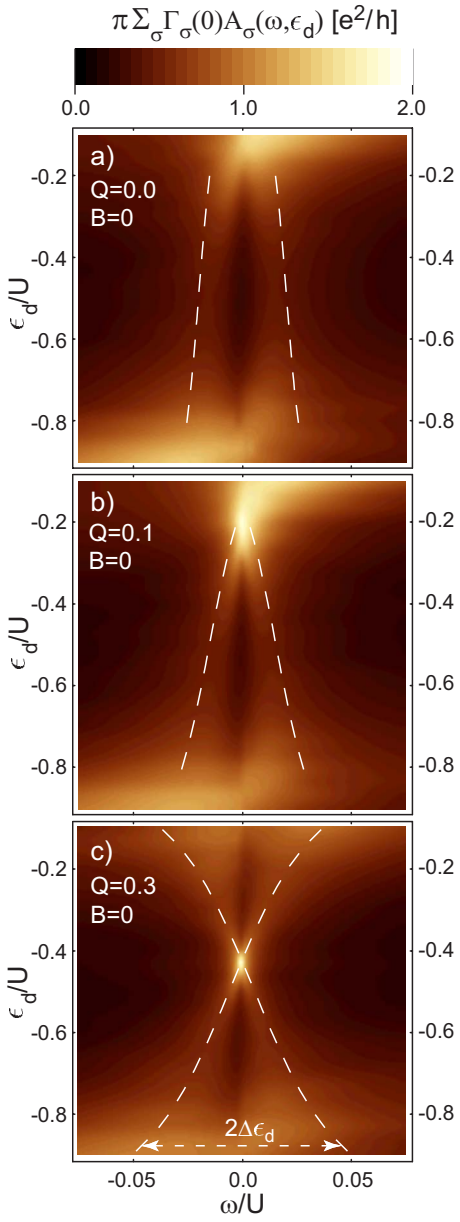

FIG. 15. (Color online) Color scale plot of the (rescaled) spectral function $\Sigma_\sigma\Gamma_\sigma A_\sigma(\omega)$: the dashed lines mark the Kondo resonance for the lead band structure as shown in Fig. 14 in the absence of an external magnetic field. Whereas panels (a)–(c) correspond to a quantum dot in the absence of an external magnetic field, in panels (d)–(f), an external field is applied.

It is interesting to consider how the Kondo resonance merges with Coulomb resonances. One can learn from Eq. (18) that the splitting $\delta\epsilon_d$ for the flat band structure without Stoner splitting shows a logarithmic divergence for $\epsilon_0\to 0$ or $U+\epsilon_0\to 0$. Since any sufficiently smooth DOS can be linearized around the Fermi surface, this logarithmic divergence occurs quite universally, as can be observed in logarithmic linear versions of Fig. 17(c) demonstrated in Fig. 18. For finite temperature ($T>0$), the logarithmic divergence for $\epsilon_0\to 0$ or $\epsilon_0\to -U$ is cut off, $\Delta\epsilon\simeq-(1/\pi)P\Gamma[\Psi(1/2)+\ln(2\pi T/U)]$, which is also important for temperatures $T\ll T_K$.

The finite slope of the Kondo resonance in the linear conductance plot motivates us to suggest an interesting possibility here. For a dot attached to leads with a DOS as described in Eq. (24) and, say, $Q=0.3$ [see Fig. 17(c)], the gate voltage can be used to tune the magnetization of the dot. In the absence of an external magnetic field $B=0$, the dot is not occupied by a preferred spin species for a particular gate voltage (which is $\epsilon_d\approx -U/2$ in this case). Consequently, the dot is preferably occupied with electrons of spin σ for $\epsilon_d\gtrsim -U/2$ and electrons of opposite spin $\bar{\sigma}$ for $\epsilon_d\lesssim -U/2$. In other words, the average spin on a dot contacted to leads with such a DOS, n_σ, and consequently its magnetization $m=n_\uparrow-n_\downarrow$, is tunable via an electric field, which, in turn, affects ϵ_d. This observation suggests the interesting possibility (similar to Ref. 44) of employing an electric field to tune the magnetic properties of a dot. To compute the gate voltage dependence of the magnetic field, of course, a detailed knowledge of the band structure in the leads is necessary. Figure 19(a) summarizes this discussion.

Another consequence of the lead band structure is that the linear conductance G does not show a plateau when plotted

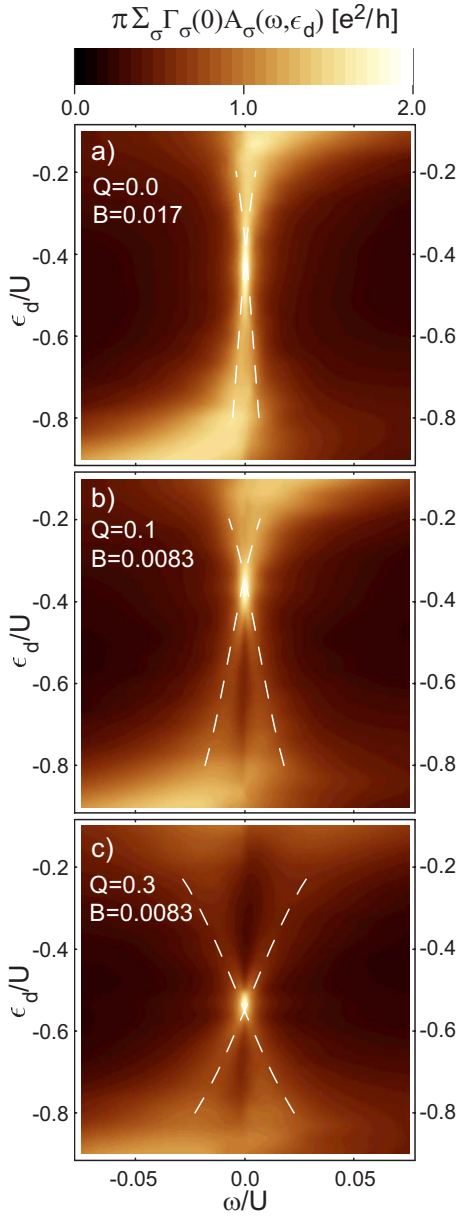

FIG. 16. (Color online) Color scale plot of the (rescaled) spectral function $\Sigma_\sigma\Gamma_\sigma A_\sigma(\omega)$: the dashed lines mark the Kondo resonance for the lead band structure as shown in Fig. 14. In contrast to Fig. 15, an external field is applied. As explained in Sec. V, a local magnetic field shifts the spin-resolved local levels relative to each other, leading to a change in the gate voltage where the compensation ($n_\uparrow = n_\downarrow$) takes place.

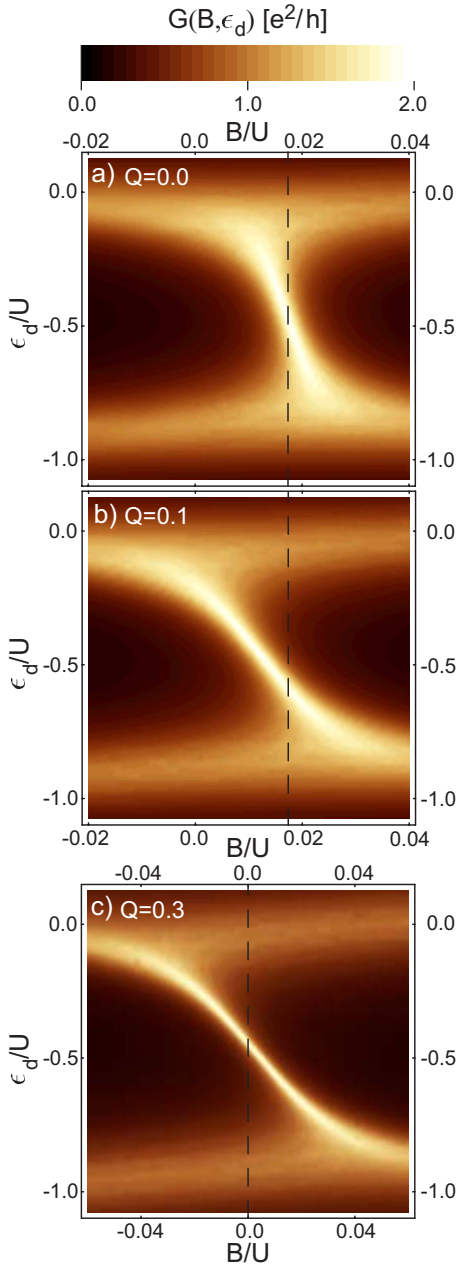

FIG. 17. (Color online) Color scale plot of the linear conductance G as a function of gate voltage ϵ_d and magnetic field B for the band structures corresponding to Figs. 14(a)–14(c) [i.e., corresponds (a) to $Q=0$, (b) to $Q=0.1$, and (c) to $Q=0.3$]. The black dashed line indicates cross sections for which the amplitude is plotted in Fig. 19(b). Note the charging resonances around $\epsilon_d \approx 0$ and $\epsilon_d \approx -U$ and the tilted resonance (due to the Kondo effect) for $-U \lesssim \epsilon_d \lesssim 0$.

relative to ϵ_d. Instead, we observe a three peak structure in G [see Fig. 19(b)] due to the particular gate voltage at which the full Kondo resonance is recovered.

The theoretical predictions made in this section were done for the particular lead DOS of Eq. (24). We used this particular lead DOS to illustrate the effects on the spin splitting of the local level triggered by the band structure of the leads. To quantitatively compare our predictions with experiments, however, a detailed knowledge of the lead DOS is necessary, which is, in general, very difficult to obtain.

VIII. CONCLUSION

We analyzed the effect of the band structure of the ferromagnetic leads on the spin splitting of the local level $\epsilon_{d\sigma}$ of a quantum dot attached to them. We analyzed the effect of a finite spin polarization P in the case of flat (energy-independent) bands. We found that the finite lead polarization results in a spin splitting of the local level and the Kondo resonance in a single-particle spectral function, which

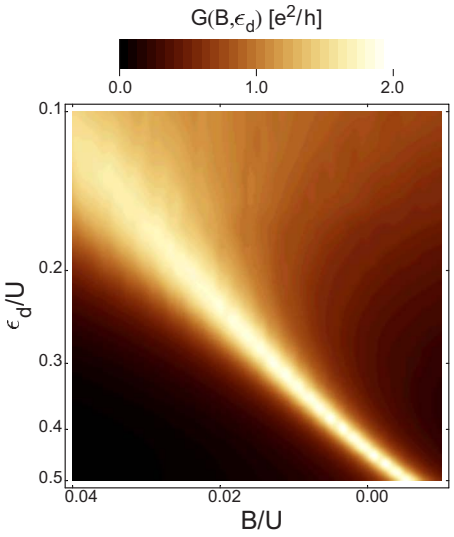

FIG. 18. (Color online) Logarithmic-linear version of Fig. 17(c). Color scale plot of the linear conductance G as a function of gate voltage ϵ_d and magnetic field B for the band structures corresponding to Fig. 14(c).

can be compensated by an appropriately tuned magnetic field. Given that the condition $n_\uparrow = n_\downarrow$ is recovered, the isotropic Kondo effect is recovered even though the dot is contacted to leads with a finite spin polarization. In Addition to this, we identified that a finite Stoner splitting introduces an effective exchange field in the dot. Finally, we explained the

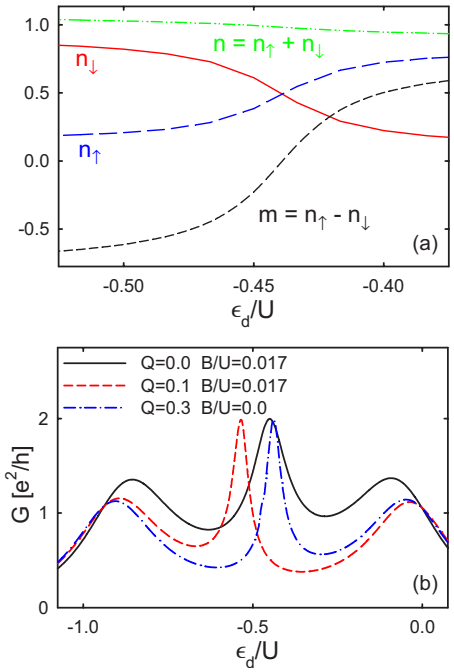

FIG. 19. (Color online) The spin-resolved impurity occupation n_σ for the DOS reflecting Figs. 14(a) and 15(a) is plotted in panel (a). It nicely illustrates that ϵ_d can be employed to tune the average impurity magnetization. Since the Kondo resonance is only fully recovered for $n_\uparrow = n_\downarrow$, the linear conductance G shows three peaks in panel (b) for three different situations corresponding to black dashed lines from Fig. 17.

consequences of an energy- and spin-dependent band structure on the local level. We confirmed that, in this general case, the Kondo resonance can also be recovered. From a methodological point of view, we extended the standard NRG procedure to treat leads with an energy- and spin-dependent DOS.

ACKNOWLEDGMENTS

We thank J. Barnaś, T. Costi, L. Glazman, W. Hofstetter, B. Jones, C. Marcus, J. Nygård, A. Pasupathy, D. Ralph, A. Rosch, Y. Utsumi, and M. Vojta for discussions. This work was supported by the DFG under the CFN, "Spintronics" RT Network of the EC RTN2-2001-00440, Projects OTKA D048665 and T048782, SFB 631, and the Polish grant for science in years 2006–2008 as a research project. Additional support from CeNS is gratefully acknowledged. L.B. is a grantee of the János Bolyai Scholarship. This research was also supported in part by the National Science Foundation under Grant No. PHY99-07949.

APPENDIX A: TRANSFORMATION OF TUNNELING HAMILTONIAN, $\hat{\mathcal{H}}_{\ell d}$

The continuous representation of the tunneling Hamiltonian $\hat{\mathcal{H}}_{\ell d}$ [Eq. (3)] can be rewritten in terms of discrete conduction band operators for each spin component separately by replacing the continuous conduction band operators $\alpha_{\omega\sigma}$ by discrete ones, as suggested in Eq. (10),

$$\hat{\mathcal{H}}_{\ell d} = \sum_{np\sigma} \left\{ d_\sigma^\dagger \left[a_{np\sigma} \int_{\Lambda^{-(n+1)}}^{\Lambda^{-n}} d\omega h_\sigma(\omega) \Psi_{np}^+(\omega) + b_{np\sigma} \int_{-\Lambda^{-n}}^{-\Lambda^{-(n+1)}} d\omega h_\sigma(\omega) \Psi_{np}^-(\omega) \right] + \text{H.c.} \right\}. \tag{A1}$$

As outlined in Sec. III, we replace the energy-dependent generalized hybridization of the nth logarithmic interval $h_\sigma(\omega)$, $\Lambda^{-(n+1)} \pm \omega < \Lambda^{-n}$, by a constant $h_{n\sigma}^\pm$, defined as

$$h_{n\sigma}^+ \equiv \begin{cases} \dfrac{1}{d_n} \displaystyle\int_{\Lambda^{-(n+1)}}^{\Lambda^{-n}} d\omega \sqrt{\rho_\sigma(\omega)[V_\sigma(\omega)]^2} & \text{if } \Lambda^{-(n+1)} \leqslant \omega < \Lambda^{-n} \\ 0 & \text{otherwise.} \end{cases}$$

$$h_{n\sigma}^- \equiv \begin{cases} \dfrac{1}{d_n} \displaystyle\int_{-\Lambda^{-n}}^{-\Lambda^{-(n+1)}} d\omega \sqrt{\rho_\sigma(\omega)[V_\sigma(\omega)]^2} & \text{if } -\Lambda^{-n} < \omega \leqslant -\Lambda^{-(n+1)} \\ 0 & \text{otherwise.} \end{cases}$$

Consequently, possible integrals in Eq. (A1), such as $\int_{\Lambda^{-(n+1)}}^{\Lambda^{-n}} d\omega h_\sigma(\omega) \Psi_{np}^+(\omega) \propto \int_{\Lambda^{-(n+1)}}^{\Lambda^{-n}} d\omega \Psi_{np}^+(\omega)$, give only a finite contribution for $p=0$ (due to the Riemann-Lebesgue lemma). For the particular choice of constant hybridization, the impurity couples to s waves ($p=0$ modes) only; consequently, we

skip the harmonic index p below. With the above definitions, Eq. (A1) simplifies to the following compact form:

$$\hat{\mathcal{H}}_{\ell d} = \frac{1}{\sqrt{\pi}} \sum_{\sigma} [d_{\sigma}^{\dagger} \sum_{n} (a_{n\sigma}\gamma_{n\sigma}^{+} + b_{n\sigma}\gamma_{n\sigma}^{-}) + \text{H.c.}], \quad \text{(A2)}$$

where

$$\gamma_{n\sigma}^{+} \equiv \int_{\Lambda^{-(n+1)}}^{\Lambda^{-n}} d\omega \sqrt{\pi \rho_{\sigma}(\omega)[V_{\sigma}(\omega)]^2},$$

$$\gamma_{n\sigma}^{-} \equiv \int_{-\Lambda^{-n}}^{-\Lambda^{-(n+1)}} d\omega \sqrt{\pi \rho_{\sigma}(\omega)[V_{\sigma}(\omega)]^2}. \quad \text{(A3)}$$

Remember that Eq. (9) forces the generalized dispersion $g_{\sigma}(\epsilon)$ to be adjusted accordingly for this particular choice of $h_{\sigma}(\omega)$. It is explained in detail in Appendix B.

APPENDIX B: MAPPING OF CONDUCTION BAND ONTO SEMI-INFINITE CHAIN

Here, we outline the important steps to bring the lead Hamiltonian $\hat{\mathcal{H}}_{\ell}$ [Eq. (8)] into the tridiagonal introduced in Eq. (13). The replacement of the continuous conduction band operators $\alpha_{\omega\sigma}$ by discrete operators [see Eq. (10)] simplifies $\hat{\mathcal{H}}_{\ell}$ significantly.[48] As shown in Ref. 27, the particular choice of the generalized hybridization function $h_{\sigma}(\omega) \to h_{n\sigma}^{\pm}$ (given in Appendix A) results in

$$\hat{\mathcal{H}}_{\ell} = \sum_{n\sigma} (\zeta_{n\sigma}^{+} a_{n\sigma}^{\dagger} a_{n\sigma} + \zeta_{n\sigma}^{-} b_{n\sigma}^{\dagger} b_{n\sigma}), \quad \text{(B1)}$$

where

$$\zeta_{n\sigma}^{+} \equiv \frac{\int_{\Lambda^{-(n+1)}}^{\Lambda^{-n}} d\epsilon \epsilon \rho_{\sigma}(\epsilon)}{\int_{\Lambda^{-(n+1)}}^{\Lambda^{-n}} d\epsilon \rho_{\sigma}(\epsilon)}, \quad \text{(B2)}$$

$$\zeta_{n\sigma}^{-} \equiv \frac{\int_{-\Lambda^{-n}}^{-\Lambda^{-(n+1)}} d\epsilon \epsilon \rho_{\sigma}(\epsilon)}{\int_{-\Lambda^{-n}}^{-\Lambda^{-(n+1)}} d\epsilon \rho_{\sigma}(\epsilon)}. \quad \text{(B3)}$$

To achieve the goal to bring $\hat{\mathcal{H}}_{\ell}$ into tridiagonal form, the tridiagonalization procedure developed by Lánczos[30] is used. In general, diagonal and off-diagonal matrix elements $\epsilon_{n\sigma}$ and $t_{n\sigma}$ (Ref. 49) need to be computed in the course of the procedure. These matrix elements can be obtained by demanding the following relation (see, e.g., Ref. 17):

$$\sum_{n\sigma} (\zeta_{n\sigma}^{+} a_{n\sigma}^{\dagger} a_{n\sigma} + \zeta_{n\sigma}^{-} b_{n\sigma}^{\dagger} b_{n\sigma}) = \sum_{n\sigma} [\epsilon_{n\sigma} f_{n\sigma}^{\dagger} f_{n\sigma} + t_{n\sigma}(f_{n\sigma}^{\dagger} f_{n+1\sigma} + f_{n+1\sigma}^{\dagger} f_{n\sigma})]. \quad \text{(B4)}$$

The spin-dependent coefficients $u_{nm\sigma}$ and $v_{nm\sigma}$ of the single-particle operator [Eq. (15)] (that acts on the nth site of the Wilson chain) $f_{n\sigma}$, given by the ansatz Eq. (14), need to be determined recursively for each spin component separately. Inverting the ansatz Eq. (14) enables one to express the discrete conduction band operators as $a_{n\sigma} = \Sigma_{m=0}^{\infty} u_{mn\sigma} f_{m\sigma}$ and $b_{n\sigma} = \Sigma_{m=0}^{\infty} v_{mn\sigma} f_{m\sigma}$, respectively. When we insert $a_{n\sigma}$ and $b_{n\sigma}$ in to the left hand side of Eq. (B4) and compare corresponding $f_{n\sigma}$ operators on both sides of this equation, we obtain

$$\sum_{m=0}^{\infty} (\zeta_{ms}^{+} u_{nm\sigma} a_{m\sigma}^{\dagger} + \zeta_{ms}^{-} v_{nm\sigma} b_{m\sigma}^{\dagger}) = \epsilon_{n\sigma} f_{n\sigma}^{\dagger} + t_{n\sigma} f_{n+1\sigma}^{\dagger} + t_{n-1\sigma} f_{n-1\sigma}^{\dagger}. \quad \text{(B5)}$$

In particular, Eq. (B5) for $n=0$ gives the following relation for the operators $f_{0\sigma}$:

$$\sum_{m=0}^{\infty} \left(\frac{\zeta_{m\sigma}^{+} \gamma_{m\sigma}^{+}}{\sqrt{\xi_{0\sigma}}} a_{m\sigma}^{\dagger} + \frac{\zeta_{m\sigma}^{-} \gamma_{m\sigma}^{-}}{\sqrt{\xi_{0\sigma}}} b_{m\sigma}^{\dagger} \right) = \epsilon_{0\sigma} f_{0\sigma}^{\dagger} + t_{0\sigma} f_{1\sigma}^{\dagger}, \quad \text{(B6)}$$

where the corresponding values of $u_{0m\sigma}$ and $v_{0m\sigma}$ [Eq. (15)] have already been inserted. Since the operators $f_{n\sigma}$ obey Fermi statistics, $\{f_{n\sigma}, f_{n'\sigma'}^{\dagger}\} = \delta_{nn'}\delta_{\sigma\sigma'}$, the anticommutator of the right hand side of Eq. (B6) with $f_{0\sigma}$ yields $\{\epsilon_{0\sigma} f_{0\sigma}^{\dagger} + t_{0\sigma} f_{1\sigma}^{\dagger}, f_{0\sigma}\} = \epsilon_{0\sigma}$. The corresponding anticommutator of the left hand side of Eq. (B6) with $f_{0\sigma}$ finally results in

$$\epsilon_{0\sigma} = \frac{1}{\xi_{0\sigma}} \sum_{m} [\zeta_{m\sigma}^{+} (\gamma_{m\sigma}^{+})^2 + \zeta_{m\sigma}^{-} (\gamma_{m\sigma}^{-})^2]. \quad \text{(B7)}$$

The initial hopping matrix element $t_{0\sigma}$ is readily obtained from the anticommutator $\{\epsilon_{0\sigma} f_{0\sigma}^{\dagger} + t_{0\sigma} f_{1\sigma}^{\dagger}, \epsilon_{0\sigma} f_{0\sigma} + t_{0\sigma} f_{1\sigma}\} = (\epsilon_{0\sigma})^2 + (t_{0\sigma})^2$. As $\epsilon_{0\sigma}$ is known, $t_{0\sigma}$ can be easily obtained from Eq. (B6),

$$(t_{0\sigma})^2 = \left\{ \Sigma_m [(\zeta_{m\sigma}^{+})^2 (\gamma_{m\sigma}^{+})^2 + (\zeta_{m\sigma}^{-})^2 (\gamma_{m\sigma}^{-})^2] - \Sigma_m [\zeta_{m\sigma}^{+} (\gamma_{m\sigma}^{+})^2 + \zeta_{m\sigma}^{-} (\gamma_{m\sigma}^{-})^2] \right\} \Big/ \xi_{0\sigma}. \quad \text{(B8)}$$

The knowledge of $\epsilon_{0\sigma}$, $t_{0\sigma}$, and $f_{0\sigma}$ now enables us to extract the coefficients of $f_{1\sigma}$ from Eq. (B6),

$$u_{1m\sigma} = \frac{\gamma_{m\sigma}^{+}}{\sqrt{\xi_{0\sigma} t_{0\sigma}}} (\zeta_{m\sigma}^{+} - \epsilon_{0\sigma}),$$

$$v_{1m\sigma} = \frac{\gamma_{m\sigma}^{-}}{\sqrt{\xi_{0\sigma} t_{0\sigma}}} (\zeta_{m\sigma}^{-} - \epsilon_{0\sigma}). \quad \text{(B9)}$$

A generalization of the argumentation above finally allows one to obtain the spin-dependent on-site energies $\epsilon_{n\sigma}$ and hopping matrix elements $t_{n\sigma}$ for the nth site of the Wilson chain,

$$\epsilon_{n\sigma} = \sum_{m} [(u_{nm\sigma})^2 \zeta_{m\sigma}^{+} + (v_{nm\sigma})^2 \zeta_{m\sigma}^{-}], \quad \text{(B10)}$$

$$(t_{n\sigma})^2 = \sum_m [(u_{nm\sigma})^2(\zeta^+_{m\sigma})^2 + (v_{nm\sigma})^2(\zeta^-_{m\sigma})^2] - (t_{n-1\sigma})^2 - (\epsilon_{n\sigma})^2, \tag{B11}$$

where the involved coefficients of the single-particle operator $f_{n+1\sigma}$, are given as

$$u_{n+1m\sigma} = \frac{1}{t_{n\sigma}}[(\zeta^+_{m\sigma} - \epsilon_{n\sigma})u_{nm\sigma} - t_{n-1\sigma}u_{n-1m\sigma}],$$

$$v_{n+1m\sigma} = \frac{1}{t_{n\sigma}}[(\zeta^-_{m\sigma} - \epsilon_{n\sigma})v_{nm\sigma} - t_{n-1\sigma}v_{n-1m\sigma}]. \tag{B12}$$

Note that it is crucial to determine the coefficients $u_{nm\sigma}$ and $v_{nm\sigma}$ even though only the matrix elements along the Wilson chain ($\epsilon_{n\sigma}$ and $t_{n\sigma}$) are finally required. The numerical solution of the above mentioned equations is rather tricky. Since the band energies are exponentially decaying in the course of the iteration, one has to use reliable numerical routines (i.e., arbitrary-precision FORTRAN routines[27]) to solve for the coefficients $u_{nm\sigma}$ and $v_{nm\sigma}$ and the matrix elements $t_{n\sigma}$ and $\epsilon_{n\sigma}$, respectively.

[1] M. R. Buitelaar, T. Nussbaumer, and C. Schönenberger, Phys. Rev. Lett. **89**, 256801 (2002).
[2] N. Sergueev, Q. F. Sun, H. Guo, B. G. Wang, and J. Wang, Phys. Rev. B **65**, 165303 (2002).
[3] P. Zhang, Q. K. Xue, Y. P. Wang, and X. C. Xie, Phys. Rev. Lett. **89**, 286803 (2002).
[4] B. R. Bulka and S. Lipiński, Phys. Rev. B **67**, 024404 (2003).
[5] R. Lopez and D. Sánchez, Phys. Rev. Lett. **90**, 116602 (2003).
[6] J. Martinek, Y. Utsumi, H. Imamura, J. Barnaś, S. Maekawa, J. König, and G. Schön, Phys. Rev. Lett. **91**, 127203 (2003).
[7] J. Martinek, M. Sindel, L. Borda, J. Barnaś, J. König, G. Schön, and J. von Delft, Phys. Rev. Lett. **91**, 247202 (2003).
[8] M. S. Choi, D. Sánchez, and R. López, Phys. Rev. Lett. **92**, 056601 (2004); P. Simon, P. S. Cornaglia, D. Feinberg, and C. A. Balseiro, Phys. Rev. B **75**, 045310 (2007).
[9] Y. Utsumi, J. Martinek, G. Schön, H. Imamura, and S. Maekawa, Phys. Rev. B **71**, 245116 (2005).
[10] A. N. Pasupathy, R. C. Bialczak, J. Martinek, J. E. Grose, L. A. K. Donev, P. L. McEuen, and D. C. Ralph, Science **306**, 86 (2004).
[11] J. Nygård, W. F. Koehl, N. Mason, L. DiCarlo, and C. M. Marcus, arXiv:cond-mat/0410467 (unpublished).
[12] S. Maekawa and T. Shinjo, *Spin Dependent Transport in Magnetic Nanostructures* (Taylor & Francis, London, 2002); *Concepts in Spin Electronics*, edited by S. Maekawa (Oxford University Press, Oxford, 2005).
[13] J. Martinek, M. Sindel, L. Borda, J. Barnas, R. Bulla, J. König, G. Schön, S. Maekawa, J. von Delft, Phys. Rev. B **72**, 121302(R) (2005).
[14] K. G. Wilson, Rev. Mod. Phys. **47**, 773 (1975).
[15] P. W. Anderson, J. Phys. C **10**, 3589 (1977).
[16] F. D. M. Haldane, Phys. Rev. Lett. **40**, 416 (1978).
[17] R. Bulla, H.-J. Lee, N.-H. Tong, and M. Vojta, Phys. Rev. B **71**, 045122 (2005).
[18] We use normalized density of statets in the leads, $\Sigma_{r\sigma}\int_{-\infty}^{\infty} d\omega \rho_{r\sigma}(\omega) = 1$, throughout this paper.
[19] L. I. Glazman and M. E. Raikh, JETP Lett. **47**, 452 (1988); T. K. Ng and P. A. Lee, Phys. Rev. Lett. **61**, 1768 (1988).
[20] W. Nolting, A. Vega, and T. Fauster, Z. Phys. B: Condens. Matter **96**, 357 (1995).
[21] E. Yu. Tsymbal and D. G. Pettifor, J. Phys.: Condens. Matter **9**, L411 (1997).
[22] We expect that a finite *s*-electron interaction, $U_s > 0$, will lead only to a slight renormalization of T_K.
[23] J. König and J. Martinek, Phys. Rev. Lett. **90**, 166602 (2003); M. Braun, J. König, and J. Martinek, Phys. Rev. B **70**, 195345 (2004); J. König, J. Martinek, J. Barnaś, and G. Schön, Lect. Notes Phys. **658**, 145 (2005).
[24] H. R. Krishna-murthy, J. W. Wilkins, and K. G. Wilson, Phys. Rev. B **21**, 1003 (1980); Phys. Rev. B **21**, 1044 (1980).
[25] T. A. Costi, A. C. Hewson, and V. Zlatic, J. Phys.: Condens. Matter **6**, 2519 (1994).
[26] W. Hofstetter, Phys. Rev. Lett. **85**, 1508 (2000).
[27] R. Bulla, Th. Pruschke, and A. C. Hewson, J. Phys.: Condens. Matter **9**, 10463 (1997).
[28] Krishna-murthy *et al.* (Ref. 24) generalized the original mapping of Wilson (Ref. 14) done for the Kondo model to a mapping of the Anderson model on the Wilson chain, still, however, with a constant lead DOS.
[29] Note that we are dealing with $V_\sigma(\omega) = V$, i.e., spin- and energy-independent tunneling matrix elements, in this section.
[30] C. Lánczos, J. Res. Natl. Bur. Stand. **45**, 255 (1950).
[31] W. Hofstetter and H. Schoeller, Phys. Rev. Lett. **88**, 016803 (2002).
[32] The spin-dependent DOS in the case of flat and spin-polarized bands (with spin-polarization parameter P) is given by $\rho_\sigma = \frac{1}{2}\rho(1 \pm P)$, where $\rho = \frac{1}{2D}$ is the corresponding normalized DOS of the full band.
[33] T. A. Costi, Phys. Rev. Lett. **85**, 1504 (2000); Phys. Rev. B **64**, 241310(R) (2001).
[34] D. C. Langreth, Phys. Rev. **150**, 516 (1966).
[35] A. C. Hewson, *The Kondo Problem to Heavy Fermions* (Cambridge University Press, Cambridge, 1993).
[36] For a single-level Anderson model, the phase of the retarded Green's function is identical to the scattering phase.
[37] Note that in the case of spin-polarized leads, the condition $n_\uparrow = n_\downarrow$ is not identical to the condition of degenerate levels, as $\Gamma_\uparrow \neq \Gamma_\downarrow$.
[38] Note that the appearance of the Stoner splitting makes the use of the generalized bandwidth D_0 ($\neq D$) necessary.
[39] These nanoparticles act as catalyst for the growth of the nanotube on the SiO_2 substrate.
[40] The value of T_K was confirmed by Nygård and Marcus (private communication).
[41] J. Paaske, A. Rosch, J. Kroha, and P. Wölfle, Phys. Rev. B **70**, 155301 (2004).
[42] To extract the equilibrium spectral function from a measurement is nontrivial as well. There have been different proposals to

achieve this. One can either use very asymmetric couplings to the leads, use a three terminal geometry [see E. Lebanon and A. Schiller, Phys. Rev. B **65**, 035308 (2002)], or extract A_{eq} from the frequency-dependent conductance or noise [see M. Sindel, W. Hofstetter, J. von Delft, and M. Kindermann, Phys. Rev. Lett. **94**, 196602 (2005)].

[43] *Handbook of the Band Structure of Elemental Solids*, edited by D. A. Papaconstantopoulos (Plenum, New York, 1986).

[44] H. Ohno, D. Chiba, F. Matsukura, T. Omiya, E. Abe, T. Dietl, Y. Ohno, K. Ohtani, Nature (London) **408**, 944 (2000); D. Chiba, M. Yamanouchi, F. Matsukura, and H. Ohno, Science **301**, 943 (2003).

[45] The DOS $\rho_\sigma(\omega)$ is defined as $\rho_\sigma(\omega)=\Sigma_k \delta(\omega-\epsilon_{k\sigma})$. Since free electrons have a dispersion $\epsilon_{k\sigma}=\frac{\hbar^2 k^2}{2m}$, one obtains $\rho_\sigma(\omega) \sim \int \sqrt{\omega'} d\omega' \, \delta(\omega-\omega')=\sqrt{\omega}$.

[46] K. Yosida, *Theory of Magnetism* (Springer, New York, 1996).

[47] We obtain the linear conductance $G(\epsilon_d,B)=\Sigma_\sigma G_\sigma(\epsilon_d,B)$ [see Eq. (23)] by computing the spin-resolved spectral function $A_\sigma(\omega=0,\epsilon_d,B)$ (for $T=0$) for those values of ϵ_d and B that are relevant for Fig. 16.

[48] M. Sindel, Ph.D. thesis, Ludwig-Maximilians-Universitat Munich, 2005.

[49] W. Hofstetter, Ph.D. thesis, Universitat Augsburg, 2000.